Clim. Past, 21, 279–297, 2025
https://doi.org/10.5194/cp-21-279-2025

Climate of the Past
Open Access
EGU

Spatial and temporal variability in sea surface temperatures and monsoon dynamics in the northwestern Arabian Sea during the last 43 kyr

Jan Maier[1,2], **Nicole Burdanowitz**[1,3], **Gerhard Schmiedl**[1,3], **and Birgit Gaye**[1,3]

[1]Institute for Geology, Universität Hamburg, Bundesstraße 55, 20146 Hamburg, Germany
[2]GeoZentrum Nordbayern, Department of Geography and Geosciences, Friedrich-Alexander University Erlangen-Nuremberg, Schlossgarten 5, 91054 Erlangen, Germany
[3]Center for Earth System Research and Sustainability (CEN), Universität Hamburg, Bundesstraße 55, 20146 Hamburg, Germany

Correspondence: Jan Maier (jan.m.maier@fau.de)

Received: 9 April 2024 – Discussion started: 2 May 2024
Revised: 22 November 2024 – Accepted: 6 December 2024 – Published: 31 January 2025

Abstract. In this study, we present the first well-dated, high-resolution alkenone-based sea surface temperature (SST) record from the northeastern Oman margin (Gulf of Oman) in the northwestern Arabian Sea. The SST reconstructions from core SL167 span the last 43 kyr and reveal temperature fluctuations of around 7 °C (ranging from 20.1 to 27.4 °C). Thus, this region has a higher sensitivity to climate variations compared to other core locations in the Arabian Sea and fills a gap in a previously unstudied region. SSTs were lowest during Heinrich event 4 (H4) and were comparatively low during H3, H2, the Younger Dryas, and the early and late Holocene. Comparatively higher SST occurred during some Dansgaard–Oeschger interstadials (D–O 11 and D–O 4–9), the Bølling–Allerød (B–A), and the mid-Holocene. The SST was predominantly influenced by the SW monsoon during warmer periods and the NE monsoon during cold intervals. Importantly, the Last Glacial Maximum stands out owing to the absence of intense cooling at the core site which clearly diverges from previously known SST patterns. We speculate that this pattern was caused by stronger NW winds and an eastward shift in the SST gradient in the Gulf of Oman, resulting in a brief and moderate cooling period. Strong SW winds during the early Holocene transported cold-water masses from the Oman upwelling into the Gulf of Oman, lowering SSTs. A rapid temperature increase of approx. 2 °C during the mid-Holocene was likely induced by the weakening of SW winds and an abrupt eastward shift in the SST gradient.

1 Introduction

The Arabian Sea is impacted by one of the world's largest and most complex climate systems – the Indian monsoon system (Gupta et al., 2020). Seasonal monsoon winds (Fig. 1) are driven by alternating atmospheric pressure gradients and induce regional and annual fluctuations in sea surface temperature (SST) patterns (Fig. 2a–d). The SW monsoon significantly influences precipitation patterns in the monsoon region, accounting for approximately 80 % of the total modern annual precipitation (Gadgil, 2003). This monsoon system also dictates environmental conditions, affecting phenomena such as droughts, floods, and terrestrial vegetation coverage. Moreover, it plays a crucial role in shaping the economies and societies of southern Asia and the Arabian Peninsula (Clift and Plumb, 2008; Krishna Kumar et al., 2004). The strength of the monsoon has undergone shifts and has changed due to past global climate variability. These monsoon fluctuations are associated with significant hydrological changes, including alternating phases of excessive and deficient precipitation, causing severe challenges for civilizations in the region (Gadgil, 2003; Krishna Kumar et al., 2004). The Indian monsoon system is an important com-

ponent of the global climate system and sustains the livelihoods of over a billion people worldwide (Gupta et al., 2020). Therefore, utilizing high-resolution paleo-reconstructions is essential for enhancing our understanding of forcing mechanisms and their impact on monsoon variability in the past, as well as improving forecasting and future climate modeling.

The last glacial period was characterized by significant climate variability in the northern North Atlantic, known as Dansgaard–Oeschger (D–O) oscillations and Heinrich events (Bond et al., 1993; Dansgaard et al., 1993; Heinrich, 1988; Johnsen et al., 1992). These oscillations are linked to instabilities in the Northern Hemisphere glacial ice sheets, resulting in a significant freshwater influx into the North Atlantic. This, in turn, impacts the Atlantic Meridional Overturning Circulation (AMOC) and can lead to a substantial reduction or even a complete shutdown (Broecker, 1994; Dansgaard et al., 1993; Ganopolski and Rahmstorf, 2001; Heinrich, 1988; Hemming, 2004; McManus et al., 2004). Building upon these insights, previous studies (e.g., Leuschner and Sirocko, 2000; Reichart et al., 1998; Sirocko et al., 1996; Schulte et al., 1999; Schulz et al., 1998) have described a strong connection between the North Atlantic Ocean and the Indian monsoon climate in the Arabian Sea during stadial (Heinrich events and Last Glacial Maximum (LGM)) and interstadial periods (D–O cycles, Bølling–Allerød (B–A), and the Holocene). To enhance our understanding of the Indian monsoon system and the identification of supraregional connections, SST reconstructions have been conducted in various regions of the Arabian Sea, as detailed in an overview by Gaye et al. (2018). Depending on the location, these reconstructions exhibited significant variations in SST (about 3 °C at maximum), responding differently to warm and cold periods, as well as local influencing factors such as atmospheric and oceanic circulations.

This study is centered around an alkenone-derived SST record (site SL167) obtained from the northeastern continental Oman margin in the Gulf of Oman in the northwestern Arabian Sea. This high-resolution sediment core spans the past 43 kyr, providing insights into the last glacial period and the transition to the current Holocene period. The new record is particularly significant since it represents the first high-resolution alkenone-derived SST record in the southeastern part of the Gulf of Oman. A compilation of SST records from the Arabian Sea by Gaye et al. (2018) showed that glacial SST was about 4 °C lower than during the Holocene. Furthermore, they argue that the general glacial SST gradient within the Arabian Sea had a stronger N–S insolation-driven component than during the Holocene with a more pronounced NW–SW circulation-driven component. However, records from the Arabian Sea show differences in the amplitude of SST changes, and SST studies from the Gulf of Oman are still completely missing. Thus, this work aims to close the gap of past SST information in the Gulf of Oman and generally complete the past SST pattern in the Arabian Sea. Previous high-resolution SST records either do not extend as far into the past (e.g., Böll et al., 2015; Huguet et al., 2006) or exhibit a lower SST resolution in the Arabian Sea (e.g., Schulte and Müller, 2001). By comparing our SST data with existing records from the Pakistan margin (site 93KL in Böll et al., 2015; site 136KL in Schulte and Müller, 2001), Oman upwelling (site MD00-2354; Böll et al., 2015), and the Horn of Africa within the Gulf of Aden (site P178-15; Tierney et al., 2016), we aim to unravel the relationship between the SW and NE monsoons within the complex Indian monsoon system. Investigating the regional SST influences in the Gulf of Oman over the past 43 kyr is crucial for advancing our comprehension of regional climatic dynamics. Additionally, we compare the obtained SST data with supraregional $\delta^{18}O$ data from the eastern Mediterranean region (Sofular Cave; Held et al., 2024) and northern high latitudes (NGRIP; Svensson et al., 2008). This comparative analysis aims to elucidate global climate impacts in the Gulf of Oman during warm and cold periods.

2 Modern climate dynamics

During the Indian summer monsoon (SW monsoon), the heating of the Asian continent (low-pressure cell) and the development of a high-pressure cell over the southern Indian Ocean lead to the development of strong, warm, and moist low-level winds from the SW direction. This drives surface ocean currents in a clockwise circulation (Somali Current and East Arabian Current) in the Arabian Sea. In contrast, with the onset of the Indian winter monsoon (NE monsoon), the pressure gradient reverses due to stronger cooling of the Tibetan Plateau (high-pressure cell) than the warmer Indian Ocean (low-pressure cell). This results in moderate, dry NE winds and a switch to a counterclockwise surface ocean circulation (Findlater, 1969; Bansod et al., 2003; Clemens et al., 1991; Clemens and Prell, 2003; Clift and Plumb, 2008; Findlater, 1969; Fleitmann et al., 2007; Schott et al., 2002; Webster et al., 1998; Webster, 2020; Wyrtki, 1973). SW monsoonal winds in spring and summer and the development of a clockwise circulation pattern induce the seasonal upwelling of cold, saline, and nutrient-rich deep-water masses through Ekman transport, especially along the eastern coasts of Oman and Somalia (De Boyer Montégut et al., 2007; Honjo et al., 1999; Izumo et al., 2008; Rixen et al., 2000). Ekman pumping lowers the SSTs in the boreal summer by about 2–3 °C on an annual average when compared to the northern, eastern, and southern Arabian Sea (Levitus and Boyer, 1994). Almost simultaneously with SW monsoon conditions, NW winds transport dust plumes predominantly from the Arabian Peninsula, as well as Iran, into the Arabian Sea and can also affect the regional SST pattern, depending on their intensity and variability (Leuschner and Sirocko, 2000; Sirocko and Sarnthein, 1989). A substantial SST gradient of 4–5 °C develops over several hundred kilometers with the onset of the SW monsoon, creating a temperature low near the coast

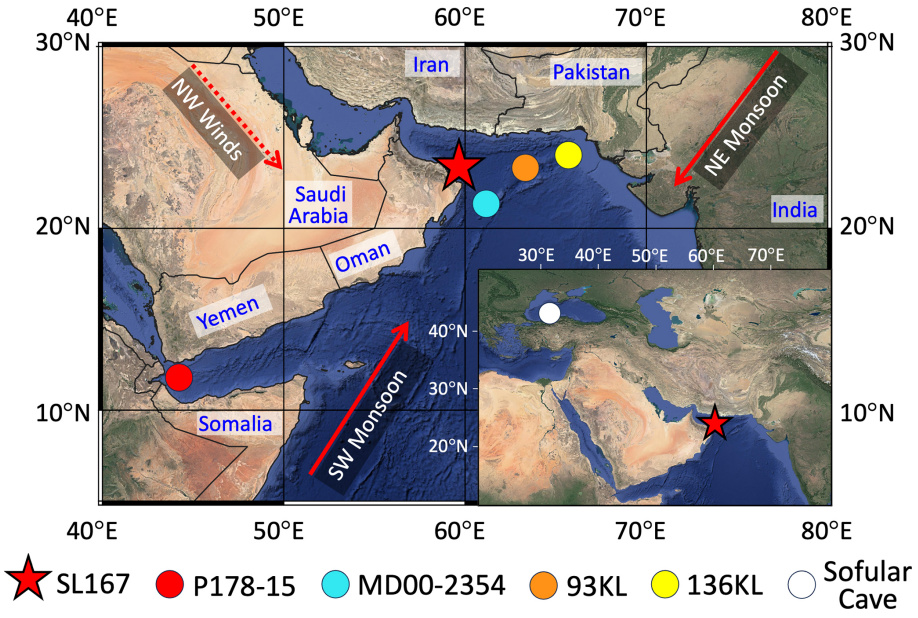

Figure 1. Map of the Arabian Sea with the location of the study site SL167 (red star) from the northwestern Arabian Sea off the Oman coast, core P178-15 (red dot) from the western Arabian Sea (Tierney et al., 2016), core MD00-2354 (blue dot) from the Oman upwelling (Böll et al., 2015), core 93KL (orange dot) from the northern Arabian Sea (Böll et al., 2015), core 136KL (yellow dot) from the northern Arabian Sea (Schulte and Müller, 2001), and the stacked record from Sofular Cave (white dot in the inset map) from northern Türkiye (Held et al., 2024). Red arrows are used to represent the dominant wind pattern during southwest (SW) monsoon and northeast (NE) monsoon. Northwesterly (NW) winds are represented by the dashed red arrow. The map was created using QGIS v 3.28.3 from © Google Earth 2024 (web map service (WMS) layer; last modification in February 2024: Google Earth, 2024) and geoBoundaries (shapefile data; last modification in February 2024: geoBoundaries, 2024).

of Oman and a high of approximately 29 °C in the western Gulf of Oman (Fig. 2c). The northern, NW, and NE Arabian Sea (north of 20° N) indicate a clear seasonal SST signal, with warmer temperatures during Northern Hemisphere summer that rapidly decrease in fall and display the lowest SSTs (ca. 23.5 °C) in the main stage of winter (Fig. 2a; Dahl and Oppo, 2006; Kumar and Prasad, 1996; Levitus and Boyer, 1994).

The Arabian Sea High-Salinity Water, Indian Ocean Central Water (IOCW), Persian Gulf Water (PGW), and Red Sea Water (RSW) constitute the four major sources of water masses in the Arabian Sea (Shetye et al., 1994). Dry air from the Himalaya during the NE monsoon causes high evaporative cooling, increases the density of surface water, and forms the Arabian Sea High-Salinity Water, particularly in the northern Arabian Sea (Kumar and Prasad, 1996, 1999; Madhupratap et al., 1996; Prasad and Ikeda, 2002; Shetye et al., 1994). The IOCW a combination of Indonesian Intermediate Water and Antarctic Intermediate Water, flows into the Arabian Sea through the SW Somali Current (500–1500 m water depths) and becomes increasingly oxygen-depleted on its way to the Arabian Sea (Emery and Meincke, 1986; Resplandy et al., 2012; You, 1998).

Postglacial sea level rise started the flooding of the Persian Gulf at around 14 ka, resulting in the transport of relatively young, warm, less oxygenated, and saline PGW through the Strait of Hormuz (25 to 70 m) into the Gulf of Oman and the Arabian Sea (Lambeck, 1996; Shetye et al., 1994). According to Beni et al. (2024), rapid transgression phases in the western Persian Gulf centered around 10.4 and 9.2 ka and have been followed by stable marine conditions since 8.8 ka. High saline PGW sinks below less saline waters and produces a salinity maximum at depths between 200 and 400 m (Bower and Furey, 2012; Pous et al., 2004; Prasad et al., 2001; Premchand et al., 1986; Shetye et al., 1994; Wyrtki, 1973). Similarly, RSW is a warm, less oxygenated, and high-saline water mass with an intermediate salinity maximum (500–1000 m water depths) in the Arabian Sea after flowing through the Strait of Bab-al-Mandeb (ca. 150 m) and mixing with the Gulf of Aden water masses (Bower et al., 2000; Pathak et al., 2021; Rochford, 1964; Wyrtki, 1973).

In the Arabian Sea, mesoscale eddies, which represent cyclonic and anticyclonic rotating water masses (Fig. 3), contrary to the surrounding main currents, emerge as key players in the regulation of surface ocean circulation (Al Saafani et al., 2007; de Marez et al., 2019; Fischer et al., 2002; Trott et al., 2019). Their upwelling and downwelling capabilities significantly affect the stratification of the upper-ocean layers through the transport and redistribution of oxygen, nutrients, salinity, and heat-driven or thermohaline water flows.

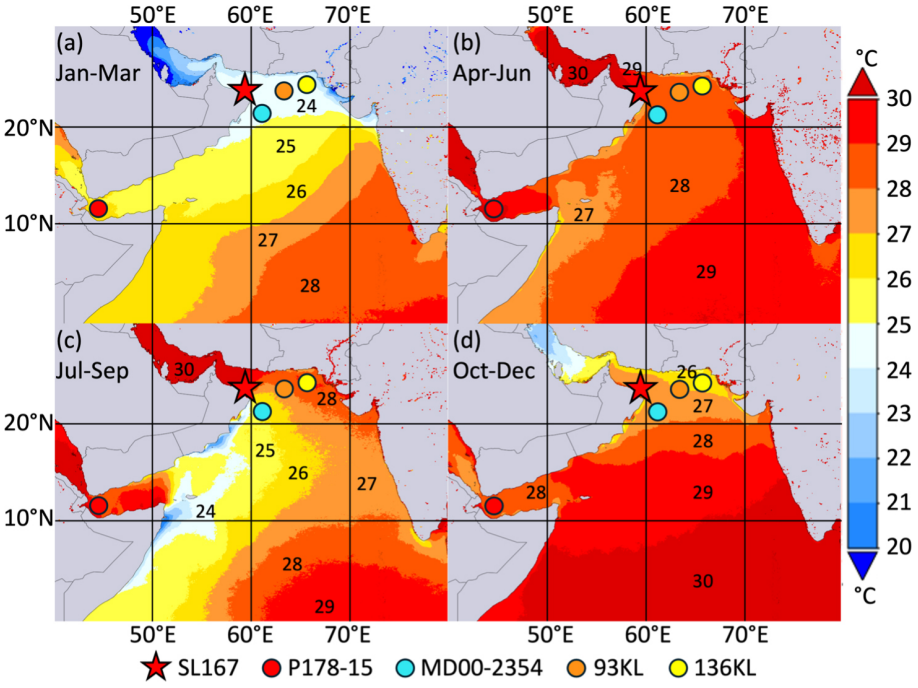

Figure 2. Map showing monthly recurring averaged SST data from 2002–2023 during **(a)** the Indian winter monsoon season (IWM; January–March). **(b)** April and June. **(c)** The Indian summer monsoon season (ISM; July–September). **(d)** October and December. Satellite date from [MODIS-Aqua MODISA_L3m_SST_Monthly_4km vR2019.0] and from Giovanni v 4.38 were used. The red star marks the location of study site SL167 in the northwestern Arabian Sea off the coast of Oman. The red dot indicates core P178-15 from the western Arabian Sea (Tierney et al., 2016). The blue dot represents core MD00-2354 from the Oman upwelling region (Böll et al., 2015). The orange dot shows core 93KL from the northern Arabian Sea (Böll et al., 2015). The yellow dot marks core 136KL from the northern Arabian Sea (Schulte and Müller, 2001).

The resulting influences on vertical and horizontal heat transport alter the regional and annual SST patterns in the Arabian Sea (Bower and Furey, 2012; Carton et al., 2012; Trott et al., 2019; Vic et al., 2015; Yao and Johns, 2010). Consequently, eddies that predominantly carry warmer waters can result in rising SSTs, while colder eddies can lead to an SST decrease. However, eddy-driven circulations are variable, transient, and continuously moving, depending on the location and seasonal climate variations (SW/NE monsoon), implying that local fluctuations in SSTs may be intense and potentially temporary (Dong et al., 2011; L'Hegaret et al., 2016; de Marez et al., 2019; Piontkovski et al., 2019; Trott et al., 2019).

3 Material and methods

The piston core SL167 (741 cm long) was collected in the northeastern part offshore of the Oman margin in the Gulf of Oman in the northwestern Arabian Sea (22°37.15′ N, 059°41.49′ E; 774 m water depth) during cruise 74/1b of research vessel (R/V) *Meteor* in September 2007 (Bohrmann et al., 2010). The core includes the period between about 3 and 43 ka. The sediment core was partitioned into sediment sample slices containing 2 cm of sediment. For the alkenone analyses, 219 freeze-dried and homogenized samples were used.

3.1 Age–depth model of core SL167

The age model published by Burdanowitz et al. (2024b) is based on 21 accelerator mass spectrometry (AMS) ^{14}C dates of surface-dwelling planktic foraminifera (Fig. 4). The Bayesian model package BACON v.2.5.6 by Blaauw and Christen (2011) in R (v.4.3; R Core Team, 2023) was used to maintain the age–depth model. Within the model, the Marine20 calibration curve and a ΔR of 93±61 years were used. For ΔR, the weighted mean of two regional marine reservoir corrections from Muscat (Southon et al., 2002) from the marine calibration database (Reimer and Reimer, 2001) was used. The age uncertainties range from ±170 to 220 years during the Holocene up to about ±770 years in the oldest part of the record (Burdanowitz et al., 2024b).

3.2 Alkenone analyses

Alkenones were measured at 2 cm of sediment for the upper 162 and 4 cm resolution below 162 cm by combining consecutive subsamples due to lower organic content (< 1.5 %). To obtain the total lipid extract (TLE), about 3 to 18 g of

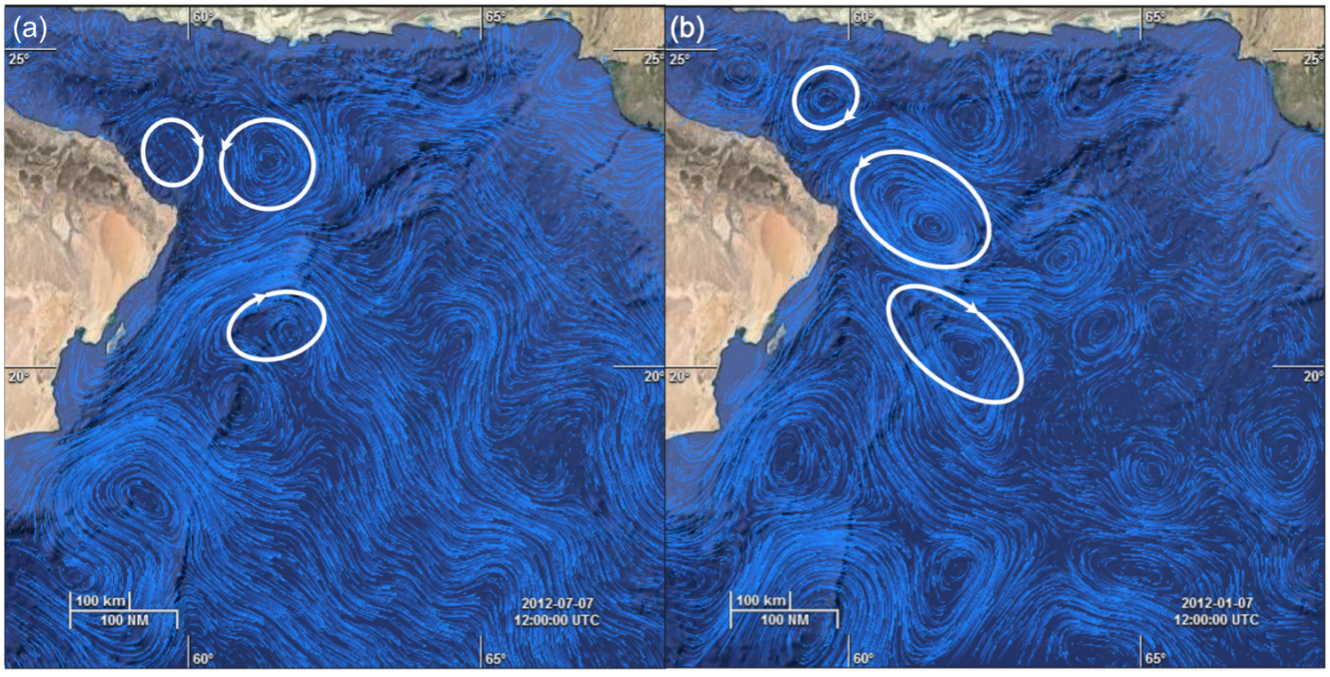

Figure 3. Snapshot of mesoscale eddies during different seasons, namely **(a)** July 2012 during the SW monsoon and **(b)** January 2012 during the NE monsoon season. Figures were generated with Ocean Data Lab (https://ovl.oceandatalab.com/, last access: 23 September 2021) using the "total 15 m current streamline (GLOBECURRENT, CMEMS)" product. The white circles with arrows denote the current streaming direction.

sediment was extracted by a Dionex Accelerated Solvent Extractor (ASE 200) using dichloromethane (DCM) and methanol (MeOH) (ratio 9 : 1) as solvent as described in Burdanowitz et al. (2024b). A known amount of an internal standard was added to the samples. During the extraction process, temperature and pressure were kept constant at 100 °C and 1000 PSI for 5 min. This procedure was performed three times. Each ASE 200 running sequence (17 to 18 cells in total) included a blank (combusted sea sand), a standard (combusted sea sand and internal standard), and a known working sediment standard. The TLEs were rotary-evaporated until almost dry. Asphaltene separation was carried out using sodium sulfate (Na_2SO_4) column chromatography for separation of the hexane-insoluble fraction. The hexane-soluble fraction was saponified with 500 µL of a 5 % potassium hydroxide solution (KOH) in MeOH and placed in the oven for 2 h at 85 °C. N-hexane was added to the saponified fraction and vortexed, followed by extraction of the upper non-mixing neutral fraction. Then the neutral fraction was separated by column chromatography into apolar, ketone (containing alkenones), and polar fractions utilizing deactivated silica gel (5 % H_2O) and different solvents (DCM for ketone separation). All samples were completely dried overnight after each preparation step.

Quantification of alkenones was carried out using a Thermo Scientific Trace 1310 gas chromatograph (GC), which used H_2 as carrier gas (35 mL min^{-1}) and is equipped with a programmable temperature vaporizer (PTV) injector (temperature 50 °C ramped with 10 °C s^{-1} to 325 °C; splitless mode) and Thermo Scientific TraceGOLD TG-5MS column (30, 0.25 mm thickness; 0.25 µm film). The GC is coupled to a flame ionization detector (FID). GC-FID was programmed to hold temperature at 50 °C for 1 min and heat to 230 °C (20 °C min^{-1}), to 260 °C (4.5 °C min^{-1}), and to 320 °C (1.5 °C min^{-1}), where the temperature is held for 15 min. Identification of $C_{37:2}$ and $C_{37:3}$ alkenones was performed by comparing peak retention times of the samples with an internal working sediment standard and was followed by quantification through integrating the peak areas of C_{37} alkenones and the internal standard (14-heptacosanone).

For the calculation of the alkenone-based unsaturation index for C_{37}-alkenones, we used the calculation by Prahl et al. (1988) as follows:

$$U^{k'}_{37} = \frac{C_{37:2}}{C_{37:2} + C_{37:3}}. \quad (1)$$

The $U^{k'}_{37}$ ratios were converted to SSTs using the regional surface calibration of the Indian Ocean (Sonzogni et al., 1997) as follows:

$$SST = \frac{U^{k'}_{37} - 0.043}{0.033}. \quad (2)$$

At the very least, duplicate measurements were performed for each sample. The analysis of the duplicate measurement indicates an average precision of 0.1 °C.

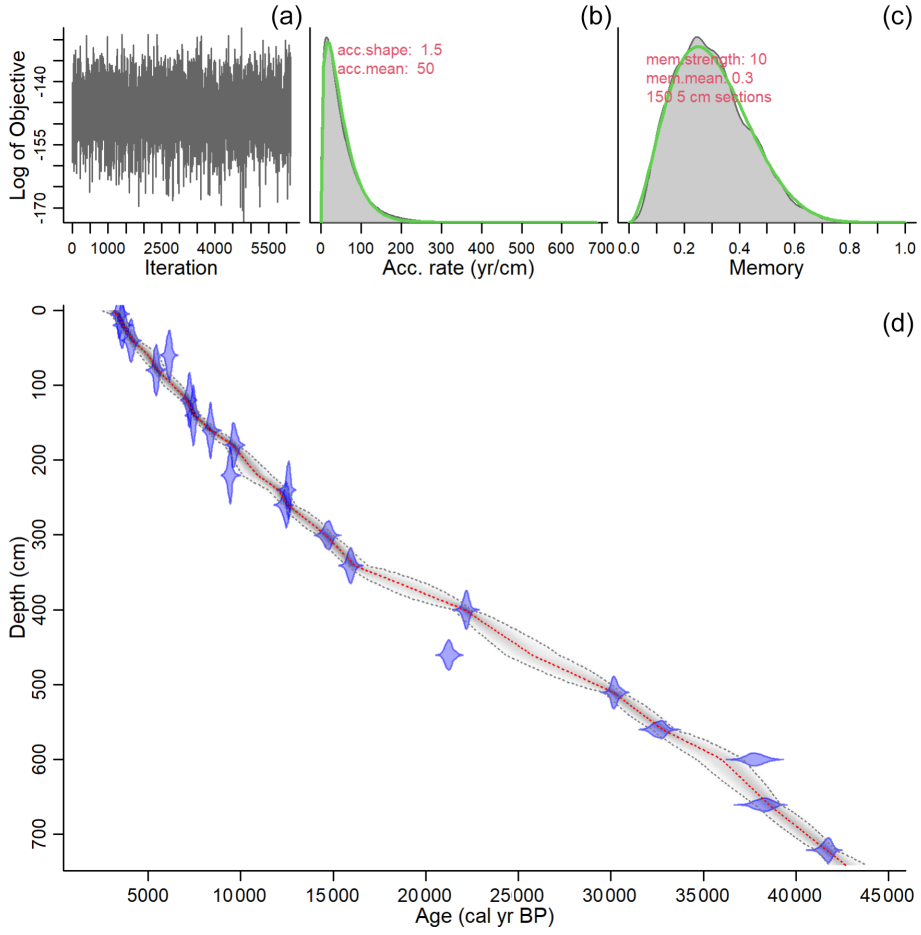

Figure 4. Age–depth model of core SL167 by Burdanowitz et al. (2024b) using the R package BACON v. 2.5.6 (Blaauw and Christen, 2011). The upper panels **(a–c)** show the Markov chain Monte Carlo iterations **(a)**, the distributions of the prior (green curve) and posterior (grey area) accumulation rates **(b)**, and memory **(c)**. The lower panel **(d)** shows the age–depth model of core SL167. The calibrated ^{14}C dates are shown in blue. The red line shows the modeled mean age of core SL167 with the 95 % confidence interval (dotted black lines). A ΔR of 93 ± 61 years was applied.

3.3 Statistical analyses

We carried out spectral and wavelet analyses in R (v.4.3; R Core Team, 2023) to identify periodicities in the reconstructed SST data set. We used the REDFIT function of the package dplR v.1.7.4 (Bunn, 2008, 2010; Bunn et al., 2022) for the spectral analysis of the reconstructed SSTs. It is based on the Fortran 90 REDFIT source code developed by Schulz and Mudelsee (2002). For the wavelet analyses, we used the R package biwavelet v.0.20.21 (Gouhier et al., 2021), using the Morlet wavelet function and bias-corrected power spectrum, which is based on Torrence and Compo (1998). The original data set has a resolution of 40 to 800 years (mean: 181 ± 124 years; median: 168 years) with the lowest resolution during the LGM (Burdanowitz et al., 2024b). Prior to the wavelet analysis, we first interpolated the reconstructed SST data to an evenly spaced data set using the package ncdf4.helpers v.0.3-6 (Bronough, 2021) and the approx. function. In detail, we used the highest resolution of the record using the function "get.f.step.size( )", resulting in a resolution of 40 years between two measurements. This results in a total of 890 time steps of an evenly spaced data set of the SL167 record.

4 Results

Alkenone-based SST record of core SL167

Based on our SST calculations using the $U^{k'}_{37}$ index, we observed a range of approx. 7 °C, ranging from 27.4 to 20.1 °C (Fig. 5a). SSTs were relatively high (26.3 to 27.4 °C) during several periods, including the mid-Holocene and periods that can be chronologically attributed to the Bølling–Allerød interstadial (B–A) and D–O interstadials 4–9 and 11. Periods of low SSTs (20.1 to 25 °C) comprise the late and early Holocene, including the 4.2 and 8.2 ka BP events. During the Pleistocene, the periods of lower SSTs can be assigned to the Younger Dryas (YD) and Heinrich events 2, 3, and 4 (H2,

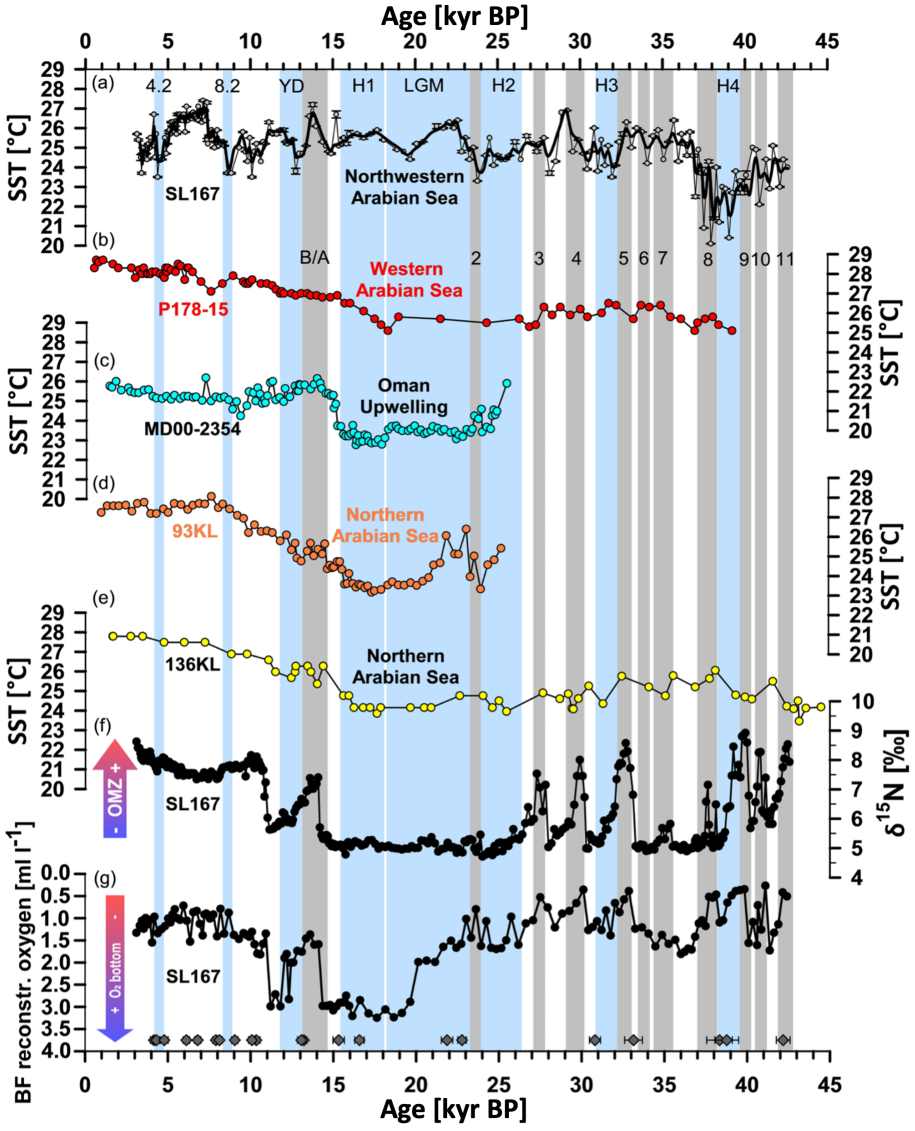

Figure 5. Contrasting SST and monsoon records in the Arabian Sea over the last 45 kyr. **(a)** SSTs of core SL167 (this study) from the northwestern Arabian Sea offshore of Oman, **(b)** core P178-15P (Tierney et al., 2016) from the western Arabian Sea, **(c)** core MD00-2354 (Böll et al., 2015) from the Oman upwelling, **(d)** core 93KL (Böll et al., 2015) from the northern Arabian Sea, and **(e)** core 136KL (Schulte and Müller, 2001) from the northern Arabian Sea. **(f)** Nitrogen isotopes (δ^{15}N; site SL167) serving as an indicator for denitrification and strength of the oxygen minimum zone (OMZ) and **(g)** the ratio of (lycopane + n-C35)/n-C31 (site SL167) indicating bottom water oxygen levels (both published in Burdanowitz et al., 2024b). Blue bars indicate the 4.2k and 8.2k events; the Younger Dryas (YD); the Last Glacial Maximum (LGM); and the Heinrich 1 (H1), Heinrich 2 (H2), Heinrich 3 (H3), and Heinrich 4 (H4) events. Timing and duration of Heinrich stadials after Allard et al. (2021). Grey bars indicate the Bølling–Allerød (B–A) interstadial and Dansgaard–Oeschger (D–O 1–D–O 11) interstadials after Fleitmann et al. (2009). Diamonds exhibit dated ages of site SL167 after Burdanowitz et al. (2024b).

H3, and H4). SSTs around the H4 (37 to 39 ka) are low but exhibit pronounced fluctuations of 3 to 4 °C. The SSTs of the LGM (18 to 23 ka) do not show significant cooling. They remain relatively warm (> 25 °C), with a short SST drop to about 24.4 °C between 19 and 20 ka. A marked increase of about 2 °C occurred during the mid-Holocene at around 7.4 ka. Spectral and wavelet analyses show significant periodicities ($\chi^2 > 95\,\%$), including a 7200-year cycle and shorter periodicities of about 525 to 401 years (Fig. 7a and b).

5 Discussion

5.1 Seasonality of SST in the Arabian Sea

Several studies from the Arabian Sea have shown that alkenone-based SST reconstructions reflect, at least for the Holocene, an annual mean temperature signal (Böll et al., 2014; Doose-Rolinski et al., 2001; Sonzogni et al., 1997). Therefore, we assume that our reconstructed SST record reflects changes in annual mean SST. Figure 2a–d illustrates the seasonal SST pattern in the Arabian Sea, highlighting the complexity and fluctuations throughout the whole year. Specifically during the winter months and the NE monsoon period, the northern Arabian Sea (sites 93KL and 136KL), including the Gulf of Oman (site SL167), cools significantly (Fig. 2a) and gradually warms up in spring (Fig. 2b) and during the SW monsoon (Fig. 2c). With the onset of fall the northern Arabian Sea gradually cools again (Fig. 2d). The SST pattern also highlights significant temperature fluctuations off the coast of Oman (site MD00-2354), with the lowest temperatures during upwelling within the SW monsoon period (Fig. 2c) but also somewhat lower SSTs in the northern part of the Oman upwelling during the winter months (Fig. 2a). The warmest SSTs in the Oman upwelling occur during the intermonsoon season in spring and fall (Fig. 2b and d). The western part of the Gulf of Aden (site P178-15) only slightly cools during the NE monsoon and otherwise shows consistently warm temperatures.

Our core location (site SL167) in the Gulf of Oman is sensitive to SST changes throughout the year due to the influence of multiple factors. These are due to the intensity of the NE and SW monsoons (Figs. 1 and 2a, c), the impact of the upwelling system along the southeast coast of Oman (Fig. 2c), the influence of mesoscale eddies and their vertical and horizontal thermohaline water flow (Fig. 3a and b), and the input from various water sources, as well as the development of a pronounced SST gradient between the Oman upwelling area and the Gulf of Oman/northern Oman margin (Fig. 2c). The movement of the SST gradient during the summer months from west to east, and vice versa, significantly impacts the local SST signal, given its spatial extent of only a few hundred kilometers (Fig. 2c). In order to differentiate the regional relationships, differences, and anomalies of the Arabian climate and monsoon cycle, we compare our SST record with other alkenone-derived SST records from different areas in the Arabian Sea (Fig. 5a–e), as well as additional regional proxy-derived climate patterns (e.g., $\delta^{18}O$ isotope data in speleothems) from the monsoon area and adjacent regions.

The overall high variations in our alkenone-based SST of up to 7 °C during the last 43 kyr (Fig. 5a) can be attributed to several climatic phases and events, which will be discussed in the following.

5.2 Sea surface temperature changes in the Gulf of Oman during the late Pleistocene and Holocene

5.2.1 SST variation during Heinrich events

The SL167 SST record indicates a sharp temperature decrease during the H4 cold event, which experienced the lowest SSTs during the past 43 kyr. Furthermore, the reconstructed SST minimum in the NW Arabian Sea marks the lowest SSTs compared with available records from the northern and western Arabian Sea (Fig. 5a–e). This temperature drop might be linked to abrupt monsoon changes with an intense NE monsoon and/or NW winds, which could cause lower SSTs at the core site within cold stages. Studies from the northwestern Arabian Sea (e.g., Sirocko and Lange, 1991; Sirocko et al., 1991) have linked increased dust loads during the last glaciation to an amplified impact of NW winds. Consequently, during the cold event, intensified NW winds may have reduced SSTs by displacing warmer surface waters and promoting vertical mixing. Simultaneously, the impact of the SW monsoon decreases due to variations in the solar radiation, resulting in a southward migration of the Intertropical Convergence Zone (ITCZ) and weakened Indian summer monsoon season (ISM; Clemens et al., 1991; Godad et al., 2022; Prell and Kutzbach, 1992; Prell and van Campo, 1986). Besides the solar insolation and the NE/SW monsoon correlation, mid-latitude westerly winds also modulate monsoon conditions. Cold events can lead to a southward shift (south of the Tibetan Plateau) and an intensification of westerly winds, resulting in an intensified NE monsoon and a fast retreat of the SW monsoon (Fang et al., 1999).

The analysis of oxygenation levels in the water column (Fig. 5f) and bottom water (Fig. 5g) from the same core reveals different impacts of the H4 event (Burdanowitz et al., 2024b). While the observed increase in the water column oxygenation corresponds with the decline in SST, the changes in bottom-water oxygenation are less marked. The simultaneous strong oxygenation of the upper water column and decreasing SST indicate a significant impact of changing atmospheric rather than oceanic currents on SST in the study region. In addition, our SST record (Fig. 5a) reveals a notable and highly fluctuating signal during and in the immediate aftermath of the H4 cold event. During this period, the SST signal is subject to a growing influence of the NE monsoon. Furthermore, enhanced SW monsoon conditions can also strongly impact the SST signal, occasionally leading to substantial fluctuations. The oxygen minimum zone (OMZ) is more developed during the H4 event compared to its lower intensity during H3, H2, and H1, when the OMZ was comparably weak (Fig. 5a and f). Note that Allard et al. (2021), which we use as a reference for the timing of Heinrich events, date the onset of H3 slightly earlier (32.7 and 31.3 ka) than the Greenland ice core records. The INTIMATE chronology (Rasmussen et al., 2014), using the nomenclature of Green-

land stadials (GSs), related GS 5.1 (around 30.6 ka) to H3 (Pedro et al., 2022), whereas GS 5.2 (around 32.0 ka) falls under the timing of H3 by Allard et al. (2021).

At the beginning of the H4 event, the OMZ in the water column was even stronger than during the D–O interstadials (see below) and the entire Holocene, while the reconstructed oxygen levels in bottom waters (Fig. 5g) were similar to the D–O interstadials. It is conceivable that during the prolonged cold phase of H4 productivity was enhanced at the core site and led to the intensification of the OMZ.

5.2.2 Dansgaard–Oeschger interstadials

Compared to the strikingly cold H4 event, higher SSTs characterize periods of moderate warming during several D–O interstadials, including D–O 11, D–O 4–D–O 9, and B–A in the NW Arabian Sea. The warm interstadials typically exhibit only a short-term increase in SST (e.g., B–A and D–O 4) and are significantly more pronounced in the northwestern Arabian Sea compared to other Arabian Sea records (Fig. 5a–e). No obvious warming trend was observed during D–O 2 and D–O 3. During the warmer interstadials, the SW monsoon intensified, while the NE monsoon weakened (Clemens et al., 1991; Prell and van Campo, 1986; Prell and Kutzbach, 1992), along with a northward shift in the ITCZ, due to a northward atmospheric energy transport across the Equator (Schneider et al., 2014). The south-to-north movement of the ITCZ during D-O interstadials is associated with an increase in solar radiation and precipitation, indicating an opposite pattern to cold events (Cheng et al., 2012; Jaglan et al., 2021). In contrast, mid-latitude westerlies lose strength during interstadials and shift northward or remain entirely north of the Tibetan Plateau (Fang et al., 1999). Furthermore, the presence of low $\delta^{18}O$ values in speleothem records from Mawmluh Cave in India indicates elevated precipitation rates and intensified SW monsoon activity during a wet phase at 33.5 and 32.5 ka (Dutt et al., 2015; Jaglan et al., 2021), occurring almost simultaneously with the D–O 6 interstadial. Recent observations suggest a direct correlation between precipitation and temperatures, suggesting increased rainfall during warm interstadials and decreased precipitation during cold stadials (Allan and Soden, 2008; Trenberth et al., 2003). Despite the short duration of the D–O warming spikes, most of them show distinctly lower oxygen concentrations in the water column and bottom water (Burdanowitz et al., 2024b).

Notably, reconstructed strong OMZ during D–O 10 and D–O 4 events at the core site (Fig. 5f; Burdanowitz et al., 2024b) are in line with somewhat lower SSTs. We attribute this to an enhanced influence of the SW monsoon winds and/or more northward-extended influence of the Oman upwelling area at the core site. Shortly after D–O 2, and with the onset of the LGM at around 23 ka, an increase in SST is observed, which could be associated with D–O 2, similar to the findings at site 93KL (Fig. 5d) and also supported by Böll et al. (2015). However, our record exhibits a distinct cold signal during D–O 2, which is even lower compared to H2, and a subsequent SST increase. Burdanowitz et al. (2024b) noted a less pronounced OMZ in the water column but sub-/anoxic conditions in the bottom water at the core site. They attributed this to an intensified inflow of oxygen-depleted RSW at intermediate depths and/or a weak inflow of Antarctic Intermediate Water into the Gulf of Oman. However, stronger winds (NW/NE winds) could have facilitated enhanced mixing and ventilation of the water column, potentially contributing to the observed ventilation differences. Note that the age uncertainty during D–O 2 is about ±350 years (Burdanowitz et al., 2024b).

5.2.3 Unusual SST pattern during the Last Glacial Maximum

Compared to other records in the Arabian Sea, the most unusual SST pattern at the core site occurred during the LGM, where SSTs do not indicate a strong cooling, except for a minimum of about 24 °C around 19 ka (Fig. 5a). The northern Arabian Sea (site 93KL and site 136KL) and the upwelling area (site MD00-2354) experienced a rapid SST drop. In contrast, the NW Arabian Sea displayed a much lower decrease in SSTs compared to site 93KL, and SSTs were not as low as observed at sites 93KL, 136KL, and MD00-2354 over the entire LGM period. Furthermore, the water column was well-ventilated during the LGM at the core site, indicated by low $\delta^{15}N$ values (Fig. 5f; Burdanowitz et al., 2024b). This phenomenon can possibly be attributed to intensified NE monsoon and NW winds, as well as weaker SW monsoon, observed in large parts of the Arabian Sea during the LGM (Burdanowitz et al., 2024b; Duplessy, 1982; Jaglan et al., 2021; Sirocko et al., 2000). The lower glacial land temperatures in central Asia (Annan and Hargreaves, 2013) and low boreal summer insolation (Böll et al., 2014, 2015; Gaye et al., 2018) resulted in an intensification of the NE monsoon and associated low SSTs. Previous studies have also sustained the hypothesis of a weakened SW monsoon during the entire glacial period (Böll et al., 2015; Naidu and Malmgren, 2005; Schulte and Müller, 2001) and may offer a potential explanation for the moderately warm SSTs observed during the entire LGM. While a prolonged winter monsoon is anticipated for the LGM, the onset and related SST reduction in the NE Arabian Sea may be postponed due to its geographical location in relation to the northern Arabian Sea. This may account for the regional annual average SST contrast between the Pakistan margin (sites 93KL and 136KL) and the Gulf of Oman (Fig. 2). Furthermore, elevated dust levels can also lead to a decrease in SST at the surface (Yue et al., 2011). However, as stronger winds and the input of dust could lower the SSTs, other factors may be responsible for the moderately warm SST at the SL167 core site. In contrast, the SST was probably also influenced by mesoscale eddies, which could have controlled the transport of warmer waters into the region during the main period of the LGM.

This eddy-driven influx likely resulted in an elevated annual mean SST compared to other locations in the Arabian Sea. Furthermore, a pronounced eastward shift in the SST gradient during this period could have also influenced the SST signal.

The lowest LGM SSTs between 19 and 20 ka at the core site are in line with other Arabian Sea records (sites P178-15, MD00-2354, and 93KL; Fig. 5b–d). However, core SL167 (Fig. 5a) shows a faster increase in SSTs right after its minimum compared to the Oman margin and northern Arabian Sea but subsequently aligns closely with the SST pattern from site P178-15P (Fig. 5b). Both temperature records display a continuous rise in SSTs, at least until the midpoint of the B–A interstadial ($\sim$ 14 ka). However, the northern Arabian Sea (sites 93KL and 136KL) and the Oman upwelling region (site MD00-2354) show a significant shift in warming, with the rise in SSTs beginning at around $\sim$ 16/17 ka. Previous studies indicate that the intensification of the ISM and weakening of the NE monsoon at the end of the LGM led to a transition from a dry phase to a wet phase during the B–A interstadial (Böll et al., 2015; Dutt et al., 2015; Herzschuh, 2006; Jaglan et al., 2021). Warming of the high latitudes and the resulting reduction in the snow cover on the Tibetan Plateau is considered to be the most dominant factor (Herzschuh, 2006; Overpeck et al., 1996; Wang et al., 2001; Zhou et al., 1999). NW winds, peaking between 15 and 13 ka (Sirocko et al., 2000), may have contributed to the earlier warming, even though SW monsoon conditions weakened (Leuschner and Sirocko, 2000; Sirocko et al., 2000). While the B–A interstadial indicates a strengthening of the SW monsoon, coastal parallel SW winds are too weak to produce upwelling, explaining the temperature increase observed in the upwelling area (site MD00-2354) after the LGM (Böll et al., 2015; Huguet et al., 2006; Saher et al., 2007). Although IOCW and RSW intermediate and deep-water masses may have had an impact on SSTs during this period, it is unlikely that their influence was substantial. This is because coccolithophores are limited to the euphotic zone (0–150 m; Baumann et al., 1999, 2005), and the IOCW and RSW occur at substantial depths.

Although SSTs in the western Arabian Sea continued the warming trend, a decline in SSTs was observed during the transition from the B–A interstadial to the YD period. An analysis of dust plumes in these regions reveals a marked reduction in dust input from the Persian Gulf but only a minor decrease in central Arabia (Sirocko et al., 2000). Consequently, NW winds may continue transporting warm air masses to central Arabia, whereas their impact on SSTs in the northern region declined. Furthermore, the cooling of the Northern Hemisphere could also have played a vital role, resulting in the strengthening of the NE monsoon and weakening of the SW monsoon (Chen et al., 1997; Dutt et al., 2015; Fuchs and Buerkert, 2008; Herzschuh, 2006; Wang et al., 2001). The synchronous SST decrease in the northern (sites 93KL and 136KL) and northwestern Arabian Sea (site SL167) during this period suggests a more substantial impact from the winter monsoon at the core site (SL167) during the YD compared to the LGM. This finding supports the hypothesis that the SST pattern may be influenced by variations in the intensity of NW winds, which can either strengthen or weaken over time. Moreover, it is worth noting that the inundation of the Persian Gulf, which began around 14 ka via the Strait of Hormuz (Lambeck, 1996), constitutes a crucial factor that must be taken into account as it likely contributed to a significant decrease in SSTs during the YD period.

5.2.4 Strong and rapid SST changes during the Holocene

Fluctuations in SSTs are much more pronounced at site SL167 compared to all the other regions of the Arabian Sea (Fig. 5a–e). While other records predominantly exhibit glacial–interglacial cycles, our record stands out for its high-amplitude millennial-scale SST oscillations. At the transition from the YD into the early Holocene, SSTs remained low (Fig. 5a). With the onset of the early Holocene, SSTs at site SL167 increasingly resembled the SST signal from the Oman upwelling (site MD00-2354). Similar SSTs from the Oman upwelling and the NW Arabian Sea are also observed during the early and late Holocene. The SST signal during the mid-Holocene exhibits a close correlation with the northern Arabian Sea cores (sites 93KL and 136KL).

In contrast, during the early Holocene, the SW monsoon intensified gradually in response to orbital forcing, i.e., intensification of summer insolation at 30° N with a maximum at around 11 ka. This was expressed in enhanced precipitation in Oman, Yemen, and south and southeast Asia (Dutt et al., 2015; Dykoski et al., 2005; Fleitmann et al., 2003, 2007; Fuchs and Buerkert, 2008; Herzschuh, 2006; Kessarkar et al., 2013). Low δ^{18}O values in speleothems indicate a rapid northward shift in the ITCZ and higher Northern Hemisphere temperatures, resulting in a stronger ISM and a weaker NE monsoon (Fleitmann et al., 2007).

The 8.2 ka cold event interrupted the warm and humid early Holocene period and weakened the ISM due to an amplified southward migration during this event of the generally northward-shifted ITCZ (Cheng et al., 2009; Dixit et al., 2014). Several studies suggested that invigorated SW monsoon winds led to a more vigorous upwelling during the early Holocene, which reflects lower SSTs and a δ^{15}N maximum (Böll et al., 2015; Rostek et al., 1997). These findings propose that strong SW winds move the water masses northward into the Gulf of Oman and affect the SST at the core site. Another study also suggested that these upwelled water masses were transported northward through gyres and eddies, affecting the oceanic stratification in the Gulf of Oman (Watanabe et al., 2017). This is supported by the lower SSTs at sites SL167 and MD00-2354 during the early and late Holocene. In response to a decrease in solar radiation, the ITCZ contin-

uously migrated southward during the mid- to late Holocene, accompanied by a continuous decrease in the SW monsoon intensity and precipitation (Fleitmann et al., 2003, 2009; Fuchs and Buerkert, 2008; Gupta et al., 2020). The hypothesis of a stronger SW monsoon at the beginning of the early Holocene is supported by a recent study from the Persian Gulf (Beni et al., 2024) and evidence of increased wind activity between 9 and 6 ka during the boreal summer (Bassinot et al., 2011). Consequently, it is plausible that during the peak of the SW monsoon at the onset of the Holocene, increased water masses were transported from the upwelling region into the Gulf of Oman (Watanabe et al., 2017) and significantly lowered SST at site SL167. However, the lowest SSTs during the early Holocene occurred between 8.5 and 8.9 ka at the core site, with a slight increase afterwards. Although the age uncertainty in our age model is around ±220 years at this time, we are convinced that the age deviation from the 8.2 ka event is not due to age uncertainty. Evidence of this is another very well dated and high-resolution alkenone-based SST record from the NE Arabian Sea (site SO90-63KA) with a similar SST pattern around that time (Burdanowitz et al., 2021).

With the beginning of the mid-Holocene, the strengthening of NE monsoon conditions likely led to a temporarily interrupted transport of upwelled water masses to the core location. However, the increasing influence of NE monsoon conditions cannot be the sole driver of the rapid increase in temperature from about 2 °C at 7.5 ka. One potential explanation for the observed changes in SST could be the inflow of water masses from the Persian Gulf into the Gulf of Oman. This hypothesis is supported by the fact that the Persian Gulf experienced increased flooding during this period and reached its present coastline at around 6 ka (Lambeck, 1996). However, the impact of PGW on the SST pattern in the Gulf of Oman may have been relatively small, given that the high-salinity PGW does not mix with the overlaying surface water, which is where the coccolithophores live (Baumann et al., 1999, 2005; Wyrtki, 1973). The strong SST gradient seems more likely to be the reason for the SST jump. An abrupt shift from a west-to-east SST gradient at approx. 7.5 ka may have increased the SST signal, followed by a gradual movement back in a westerly direction, resulting in a slow decrease in surface temperature.

The upwelling region exerted an increased influence from 5 ka onwards, evident from similar SST signals in the Gulf of Oman (core SL167) and the Oman upwelling area (site MD00-2354), and suggests that an increased influx of upwelling water masses could have gradually shifted the SST gradient back to a westerly direction. Beni et al. (2024) also argue that the NE monsoon became dominant after 6 ka. Consequently, it is plausible that the interplay between weakening SW winds (Bassinot et al., 2011) and a gradually strengthening NE monsoon abruptly prevented the transport of cold-water masses from the upwelling region into the Gulf of Oman, preventing a further decrease in SST.

The decline in SSTs by about 5 ka also coincides closely with the transition to the end of the mid-Holocene Climate Optimum period that also falls within the end of the African Humid Period (Dallmeyer et al., 2013; Herzschuh, 2006), suggesting a possible connection between these phenomena. However, the Sahara did not dry out rapidly and consistently. While abrupt changes are observed in some areas (Demenocal et al., 2000; Tierney and Demenocal, 2013), other regions experienced a gradual stepwise drying, emphasizing the nonlinearity of the hydroclimate (Dallmeyer et al., 2020; Tierney et al., 2017). Similarly, Fleitmann et al. (2007) excluded an abrupt weakening of the monsoon precipitation during the mid-Holocene in the monsoon region. While a definitive connection cannot be proven, it also cannot be ruled out. However, it is more likely that the aforementioned processes played a more significant and influential role in shaping the observed changes.

During the mid- to late Holocene transition period, the SST record captures a pronounced 4.2 ka BP event. Despite the prevailing aridity in significant parts of western Asia during this period (Giesche et al., 2019), SSTs demonstrate substantial variability throughout the transition and late Holocene. Consequently, as the SSTs fluctuate considerably, it becomes challenging to establish a conclusive link between an SST drop and the 4.2 ka event.

Overall, even during the Holocene, it becomes evident that we observe strong SST variations, with the cold events of 4.2 ka and 8.5 to 8.7 ka standing out as particularly significant signals with minor uncertainties surrounded by multiple SST fluctuations. This phenomenon could be attributed to several potential factors. The unique geographical and topographic features of the core site location in the Gulf of Oman may render it more sensitive to atmospheric and oceanographic changes, including pronounced local oceanographic processes such as currents and upwelling. Additionally, the region's geographic location and exposure could amplify the impacts of weather events such as storms or strong winds. The coastal features and topography of the Gulf of Oman could also contribute to faster warming or cooling of the water, particularly in shallower areas or near landmasses. Finally, alterations in ocean circulation patterns specific to the Gulf of Oman may result in increased SST variability by affecting the distribution of warm and cold water.

5.3 Potential global drivers of SST variations in the Gulf of Oman

The SL167 SST record exhibits periodic fluctuations consistent with millennial-scale oscillations yet diverges from glacial and interglacial changes. Notably, it demonstrates remarkable similarities extending beyond the Arabian Sea, as evidenced by ice core data from Greenland (Fig. 6a; Svensson et al., 2008) and $\delta^{13}C$ time series of cave carbonates from the Mediterranean region (Fig. 6b; Held et al., 2024). Most periods of lower SSTs (e.g., during YD and Heinrich events)

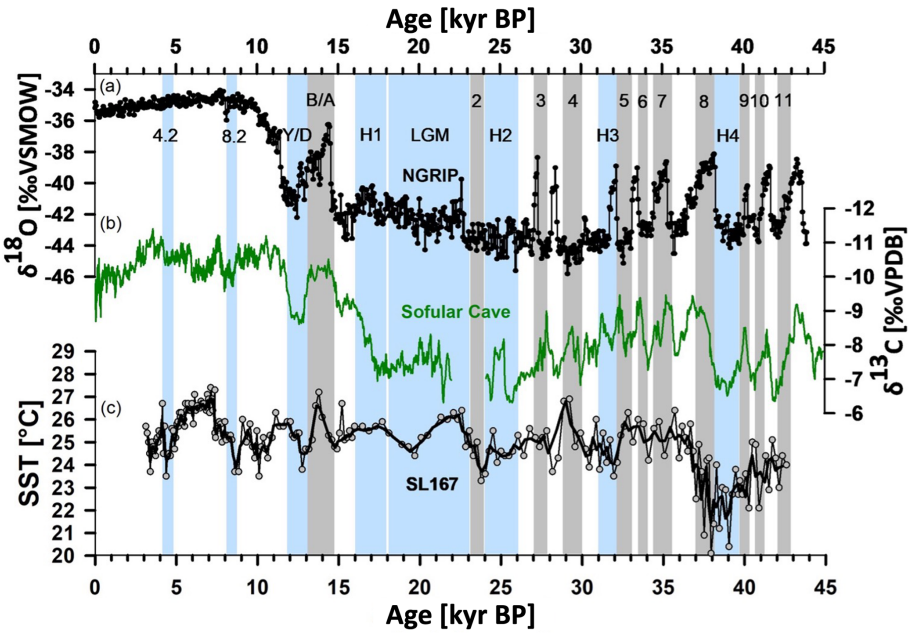

Figure 6. **(a)** NGRIP δ^{18}O time series, derived from the northern Greenland ice core (Svensson et al., 2008). **(b)** δ^{13}C and time series of a stacked record from Sofular Cave in northwestern Türkiye (Held et al., 2024). **(c)** Alkenone-derived SSTs of core SL167 (this study) from the northwestern Arabian Sea. Blue bars indicate the Younger Dryas (YD); Last Glacial Maximum (LGM); and the Heinrich 1 (H1), Heinrich 2 (H2), Heinrich 3 (H3), and Heinrich 4 (H4) events. Grey bars indicate the Bølling–Allerød (B–A) interstadial and Dansgaard–Oeschger (D–O 1–D–O 11) interstadials after Fleitmann et al. (2009).

in the NW Arabian Sea correlated with enhanced δ^{18}O values from the North Greenland Ice Core Project (NGRIP), indicating cold-air temperatures in Greenland and the northern North Atlantic. Conversely, higher SSTs (e.g., during D–O interstadials) correlated with several lower δ^{18}O values are characterized by moderate interstadial events in the North Atlantic Ocean. Based on these findings, it can be inferred that the area of our core location is not exclusively shaped by local factors but rather responsive to global temperature fluctuations that affect the SST signal.

Several studies have already suggested a close linkage between the North Atlantic Ocean, the AMOC, and the Indian monsoon climate in the Arabian Sea based on the climate variability in the D–O cycles and Heinrich events (Leuschner and Sirocko, 2000; Reichart et al., 1998; Schulte et al., 1999; Schulz et al., 1998; Sirocko et al., 1996). A weakening (strengthening) of the AMOC, e.g., around the 8.2 ka cold event (or reverse with D-O interstadials), caused a southward (northward) shift in the ITCZ, which also suggests a decrease (increase) in the ISM (Cheng et al., 2009; Deplazes et al., 2014; Krebs and Timmermann, 2007; Zhang and Delworth, 2005). Although the monsoon strength is obviously linked to the North Atlantic and occasionally responds vigorously to abrupt climatic events (e.g., H4), the SST record of core SL167 does not reflect all warm or cold periods (e.g., no prominent cooling during the LGM). These findings demonstrate that Northern Hemisphere cooling may influence the strength of the SW/NE monsoon and SSTs, but other oceanic and atmospheric factors (mesoscale eddies, strong SST gradient, and NW winds) can also have a crucial impact.

To identify any cyclic patterns in the Gulf of Oman SST record and gain insights into the influencing factors, we conducted spectral (Fig. 7a) and wavelet analyses of SST data (Fig. 7b). The spectral analysis revealed significant periodicities of 7200 years ($\chi^2 > 95\,\%$) in the SST data. This period could potentially be attributed to Heinrich events, which are characterized by large-scale melting of the Laurentide ice sheet and abrupt climate changes occurring over approximately 6.1 ka (Mayewski et al., 1997) and 7.0 ka (Calov et al., 2002). The alignment of our SST data with these periods obtained through spectral analysis supports this hypothesis. However, the wavelet analysis indicates that the prevalence of this period is not entirely evident, particularly during the interval from approx. 11–19 ka. Instead, this periodicity could potentially be attributed to oscillations in atmospheric ^{14}C, as suggested by Southon (2002). Their findings provide a rationale for the occurrence of archaeomagnetic coincidences within a 7 ka cycle, which is influenced by fluctuations in geomagnetic shielding as modulated by ^{14}C data. The 7200-year cycle may also be a subharmonic of the precession cycle, which was also suggested by Naidu et al. (2019).

Additionally, the spectral analysis revealed the presence of cycles of 7550, 4950, 3750, 2200, and 950 year BP within the

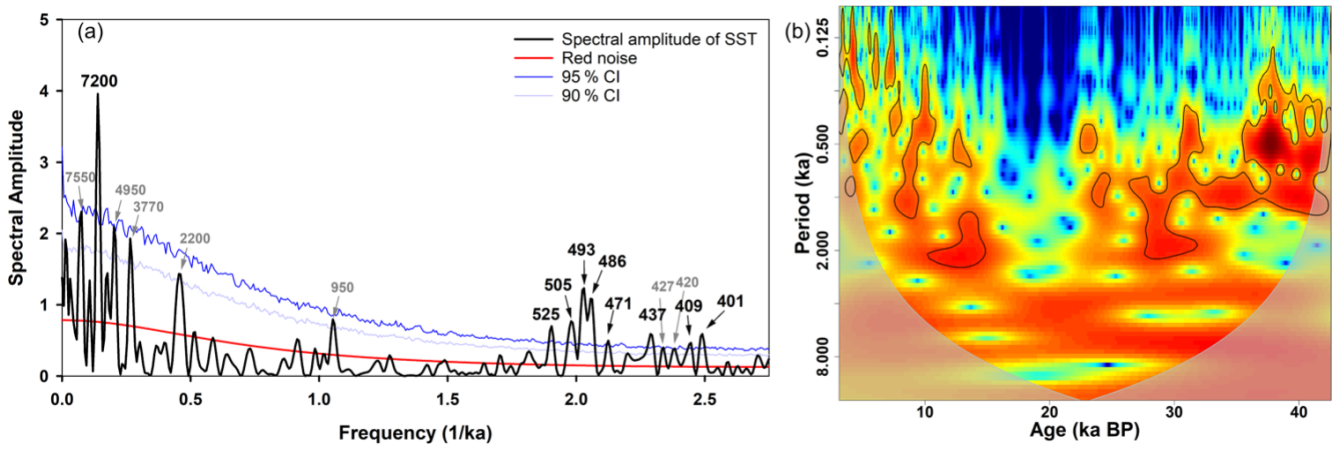

Figure 7. Spectral analyses **(a)** of the SST amplitude of core SL167 (spectral amplitudes given in years and frequencies in 1 ka^{-1}). The shaded grey area shows the cone of influence, and red (blue) colors represent the high (low) power of the wavelet power spectrum. The black line denotes the 95 % significance level. The wavelet analysis visualization **(b)** depicts the time frequency profile of a signal through wavelet transformation, featuring various signal characteristics distinguished by colors, offering insights into the temporal- and frequency-related aspects of the analyzed signals. The blue line represents the cone of influence, while the black lines denote the 95 % significance level.

90 % confidence interval ($\chi^2 > 90$ %) as well. The presence of a 2200-year periodicity in monsoons was first observed in sediment records obtained off the coast of Oman (Naidu and Malmgren, 1995). This periodicity was attributed to interactions between oceanic circulation, atmospheric carbon fluctuations (Naidu and Malmgren, 1995; Thamban et al., 2007), and solar activity as estimated by tree-ring records (Lean, 2002; Struiver and Brazinuas, 1993; Thamban et al., 2007). Our wavelet analysis reveals the presence of this cycle within the time intervals of ca. 18–5 and 35–22 ka. The remarkable reduction in cyclicity between 22 and 18 kyr BP, reflects stable LGM conditions and is a characteristic feature of this record which requires further investigation in the future. At the periodicity of 950 years, a widespread cycle emerges, supported by stalagmites from Oman (Neff et al., 2001), lake sediments from Alaska (Sheng Hu et al., 2003), and ^{14}C tree-ring data from the Northern Hemisphere (Lean, 2002). These findings strongly indicate a primary solar influence on this cycle (Lean, 2002; Neff et al., 2001; Sheng Hu et al., 2003; Thamban et al., 2007).

The results of the spectral analysis indicate the presence of periodicities of 525, 505, 493, 486, 471, 437, 409, and 401 years ($\chi^2 > 95$ %), as well as 427 and 420 years ($\chi^2 > 90$ %), in our data set. These relatively short periodicities are predominantly present in the Holocene and have been observed and documented in global records. Thus, several studies, such as the analysis of ^{14}C tree rings (Struiver and Brazinuas, 1993), demonstrate that the 500-year periodicity is attributed to changes in ocean circulation, especially of the Atlantic deep-water formation (Bhushan et al., 2001; Kessarkar et al., 2013). Considering the close relationship between Asian monsoons and the position of the ITCZ, the 500-year periodicity could be closely linked (Kessarkar et al., 2013). The other periodicities also appear to be associated with solar cycles (Menzel et al., 2014). Loutre et al. (1992) suggest that cycles of 432 years (88 % probability) correspond to eccentricity periodicities; thus, at least the 437-year cycle in our data set can be attributed to them. Although there are some differences in the other cycles (±30 years), the possibility of a correlation should not be disregarded. However, it is important to note that the resolution of these numerous short periods is not very precise (Fig. 7b). This is particularly evident around and during the LGM (approx. 15–23 ka), where no clear periodicity can be identified. Such gaps may reflect chronological uncertainties and resolution limits in this part of the record. Furthermore, these short periods can potentially be assigned to the cyclicity peaks but could also reflect inherent uncertainties in the age model, which range from 170–240 years for the Holocene and up to 770 years for the oldest part of the record.

6 Conclusion

In this study, we present a high-resolution alkenone-based SST record from the Gulf of Oman spanning the past 43 kyr. The SST reveals significant temperature fluctuations of about 7 °C, reflecting diverse climatic influences and demonstrating increased sensitivity to climate variations compared to other Arabian Sea core locations. Thus, we provide the first SST data from this unique region and further complete the SST pattern in the Arabian Sea. The most prominent cold phase occurred during the H4 event with SSTs down to about 21 °C. Further cooler SST phases are reconstructed during the H3 event, which is the period between 19 and 20 ka, and YD, as well as the 8.2 and 4.2 ka events. We attribute these SST declines to reduced solar radiation and a southward

ITCZ shift from a weakened AMOC, leading to strengthened mid-latitude westerlies and NE monsoon conditions while weakening the SW monsoon. Conversely, SSTs remain warm during D–O 11, D–O 4–9, and B–A, marked by increased solar radiation and a northward ITCZ shift that intensifies the SW monsoon and weakens NE monsoon conditions.

One of the most striking features of our record is the absence of a strong SST decrease during the LGM, which is markedly distinct from previous SST reconstructions in the Arabian Sea, where a more pronounced drop was consistently observed. This may be linked to a weakened SW monsoon and a reinforced NE monsoon. Yet, enhanced NW winds, warmer eddy currents, and an SST gradient shift in the Gulf of Oman significantly influence SSTs during this cold period. Compared to other Arabian Sea SST records, our record reveals strong rapid SST fluctuations throughout the Holocene by about 4 °C. The 8.5–8.7 and 4.2 ka events are marked as cold-SST events at the core location. Furthermore, a strong and rapid increase in SSTs of about 3.5 °C within about 1200 years during the mid-Holocene SST may be attributed to an abrupt eastern shift in the SST gradient.

The SL167 SST record highlights the sensitivity of the Gulf of Oman to climatic variations. Specifically, it emphasizes the complex interaction of monsoonal and oceanographic processes influencing SST variations due to the unique semi-enclosed location at the gateway of the Gulf of Oman and the Arabian Sea. The location of the Gulf of Oman makes it an important area for understanding the general climatic mechanisms in the region. Future research, particularly in the Gulf of Oman, is essential to better understand the complexity of this system. Additionally, placing these findings within a broader regional framework, which includes neighboring marine and atmospheric systems, will improve our understanding of past climate/oceanic dynamics. This approach will help to reveal how changes in the Gulf of Oman influenced and were influenced by larger climate patterns in the Indian Ocean and surrounding areas.

Data availability. The alkenone-based SST data set is stored and available at PANGAEA under https://doi.org/10.1594/PANGAEA.967645 (Burdanowitz et al., 2024a).

Author contributions. JM: conceptualization, formal analysis, investigation, methodology, visualization, and writing (original draft preparation). NB: conceptualization, formal analysis, investigation, methodology, visualization, and writing (original draft preparation). GS: conceptualization, resources, supervision, and writing (original draft preparation). BG: conceptualization, supervision, and writing (original draft preparation).

Competing interests. The contact author has declared that none of the authors has any competing interests.

Disclaimer. Publisher's note: Copernicus Publications remains neutral with regard to jurisdictional claims made in the text, published maps, institutional affiliations, or any other geographical representation in this paper. While Copernicus Publications makes every effort to include appropriate place names, the final responsibility lies with the authors.

Acknowledgements. This research has been funded by the Deutsche Forschungsgemeinschaft (DFG, German Research Foundation) through Germany's Excellence Strategy – EXC 2037 "CLICCS – Climate, Climatic Change, and Society" – project no. 390683824, as part of the contribution to the Center for Earth System Research and Sustainability (CEN) at Universität Hamburg. The monthly SST visualizations used in this paper were produced with the Giovanni online data system developed and maintained by the NASA Goddard Earth Sciences Data and Information Services Center (GES DISC). We acknowledge and appreciate their contribution to the availability and accessibility of valuable data for our research. We extend our thanks to Ocean Data Lab for supplying the mesoscale eddy data utilized in this paper. We thank Hartmut Schulz for his support during core recovery and sampling. We express our gratitude to Frauke Langenberg, Marc Metzke, Miriam Warning, and Sabine Beckmann for providing technical and analytical support. Furthermore, we thank the three anonymous reviewers for their constructive and helpful comments which helped us to improve the paper.

Financial support. This research has been supported by the Deutsche Forschungsgemeinschaft (grant no. 390683824).

Review statement. This paper was edited by Luc Beaufort and reviewed by three anonymous referees.

References

Allan, R. P. and Soden, B. J.: Atmospheric warming and the amplification of precipitation extremes, Science, 1481–1484, https://doi.org/10.1126/science.1160787, 2008.

Allard, J. L., Hughes, P. D., and Woodward, J. C.: Heinrich Stadial aridity forced Mediterranean-wide glacier retreat in the last cold stage, Nat. Geosci., 14, 197–205, https://doi.org/10.1038/s41561-021-00703-6, 2021.

Al Saafani, M. A., Shenoi, S. S. C., Shankar, D., Aparna, M., Kurian, J., Durand, F., and Vinayachandran, P. N.: Westward movement of eddies into the Gulf of Aden from the Arabian Sea, J. Geophys. Res.-Oceans, 112, C11004, https://doi.org/10.1029/2006JC004020, 2007.

Annan, J. D. and Hargreaves, J. C.: A new global reconstruction of temperature changes at the Last Glacial Maximum, Clim. Past, 9, 367–376, https://doi.org/10.5194/cp-9-367-2013, 2013.

Bansod, S. D., Yin, Z. Y., Lin, Z., and Zhang, X.: Thermal field over Tibetan Plateau and Indian summer monsoon rainfall, Int. J. Climatol., 23, 1589–1605, https://doi.org/10.1002/joc.953, 2003.

Bassinot, F. C., Marzin, C., Braconnot, P., Marti, O., Mathien-Blard, E., Lombard, F., and Bopp, L.: Holocene evolution of summer

winds and marine productivity in the tropical Indian Ocean in response to insolation forcing: Data-model comparison, Clim. Past, 7, 815–829, https://doi.org/10.5194/cp-7-815-2011, 2011.

Baumann, K.-H., Cepek, M., and Kinkel, H.: Coccolithophores as indicators of ocean water masses, surface-water temperature, and paleoproductivity examples from the South Atlantic, in: Use of Proxies in Paleoceanography: Examples from the South Atlantic, edited by: Fischer, G. and Wefer, G., Springer, Berlin, Heidelberg, 117–144, https://doi.org/10.1007/978-3-642-58646-0_4, 1999.

Baumann, K.-H., Andruleit, H., Bockel, B., Geisen, M., and Kinkel, H.: The significance of extant coccolithophores as indicators of ocean water masses, surface water temperature, and palaeoproductivity: a review, Palaontol. Z., 7, 31–34, 2005.

Beni, A. N., Leduc, G., Djamali, M., Sharifi, A., Marriner, N., Tachikawa, K., Rostek, F., Tjallingii, R., Lahijani, H., Arabshahi, M. M., Garcia, M., Licari, L., Tetard, M., Bellinghery, M. C., and Bard, E.: Postglacial flooding and Holocene climate shifts in the Persian Gulf, J. Quaternary Sci., 39, 592–607, https://doi.org/10.1002/jqs.3614, 2024.

Bhushan, R., Dutta, K., and Somayajulu, B. L. K.: Concentrations and burial fluxes of organic and inorganic carbon on the eastern margins of the Arabian Sea, Mar. Geol., 178, 95–113, 2001.

Blaauw, M. and Christen, J. A.: Flexible paleoclimate age-depth models using an autoregressive gamma process, Bayesian Anal., 6, 457–474, https://doi.org/10.1214/11-BA618, 2011.

Bohrmann, G., Lahajnar, N., Gaye, B., Spieß, V., and Betzler, C.: Nitrogen cycle, cold seeps, carbonate platform development in the Northwestern Indian Ocean, Cruise No. 74, 31 August–22 December 2007, METEOR-Berichte, Leitstelle Meteor, Institut für Meereskunde der Universität Hamburg, 1–212, https://doi.org/10.2312/cr_m74, 2010.

Böll, A., Lückge, A., Munz, P., Forke, S., Schulz, H., Ramaswamy, V., Rixen, T., Gaye, B., and Emeis, K. C.: Late Holocene primary productivity and sea surface temperature variations in the northeastern Arabian Sea: Implications for winter monsoon variability, Paleoceanography, 29, 778–794, https://doi.org/10.1002/2013PA002579, 2014.

Böll, A., Schulz, H., Munz, P., Rixen, T., Gaye, B., and Emeis, K. C.: Contrasting sea surface temperature of summer and winter monsoon variability in the northern Arabian Sea over the last 25 ka, Palaeogeogr. Palaeoclim. Palaeoecol., 426, 10–21, https://doi.org/10.1016/j.palaeo.2015.02.036, 2015.

Bond, G., Broecker, W., Johnsen, S., McManus, J., Labeyrie, L., Jouzel, J., and Bonani, G.: Correlations between climate records from North Atlantic sediments and Greenland ice, Nature, 365, 143–147, 1993.

Bower, A. S. and Furey, H. H.: Mesoscale eddies in the Gulf of Aden and their impact on the spreading of Red Sea Outflow Water, Prog. Oceanogr., 96, 14–39, https://doi.org/10.1016/j.pocean.2011.09.003, 2012.

Bower, A. S., Hunt, H. D., and Price, J. F.: Character and dynamics of the Red Sea and Persian Gulf outflows, J. Geophys. Res.-Oceans, 105, 6387–6414, https://doi.org/10.1029/1999jc900297, 2000.

Broecker, W. S.: Massive iceberg discharges as triggers for global climate change, Nature, 372, 421–424, 1994.

Bronough, D.: ncdf4.helpers: Helper Functions for Use with the "ncdf4" Package, R package version 0.3-6, CRAN [code], https://cran.r-project.org/package=ncdf4.helpers (last access: 8 August 2023), 2021.

Bunn, A., Korpela, M., Biondi, F., Campelo, F., Mérian, P., Qeadan, F., and Zang, C.: dplR: Dendrochronology Program Library in R, R package version 1.7.4, CRAN [code], https://cran.r-project.org/package=dplR (last access: 27 June 2023), 2022.

Bunn, A. G.: A dendrochronology program library in R (dplR), Dendrochronologia, 26, 115–124, https://doi.org/10.1016/j.dendro.2008.01.002, 2008.

Bunn, A. G.: Statistical and visual crossdating in R using the dplR library, Dendrochronologia, 28, 251–258, https://doi.org/10.1016/j.dendro.2009.12.001, 2010.

Burdanowitz, N., Rixen, T., Gaye, B., and Emeis, K. C.: Signals of Holocene climate transition amplified by anthropogenic land-use changes in the westerly-Indian monsoon realm, Clim. Past, 17, 1735–1749, https://doi.org/10.5194/cp-17-1735-2021, 2021.

Burdanowitz, N., Maier, J., Gaye, B., and Schmiedl, G.: Alkenone-based sea surface temperature reconstruction of sediment core GeoTü SL167 [dataset], PANGEA [data set], https://doi.org/10.1594/PANGAEA.967645, 2024a.

Burdanowitz, N., Schmiedl, G., Gaye, B., Munz, P. M., and Schulz, H.: Distinct oxygenation modes of the Gulf of Oman over the past 43 000 years – a multi-proxy approach, Biogeosciences, 21, 1477–1499, https://doi.org/10.5194/bg-21-1477-2024, 2024b.

Calov, R., Ganopolski, A., Petoukhov, V., Claussen, M., and Greve, R.: Large-scale instabilities of the Laurentide ice sheet simulated in a fully coupled climate-system model, Geophys. Res. Lett., 29, 2216, https://doi.org/10.1029/2002GL016078, 2002.

Carton, X., L'Hegaret, P., and Baraille, R.: Mesoscale variability of water masses in the Arabian Sea as revealed by ARGO floats, Ocean Sci., 8, 227–248, https://doi.org/10.5194/os-8-227-2012, 2012.

Chen, F. H., Wang, J. M., Li, J. J., and Oldfield, F.: High-resolution multi-proxy climate records from Chinese loess: evidence for rapid climatic changes over the last 75 kyr, Palaeogeogr. Palaeoclim. Palaeoecol., 130, 323–335, 1997.

Cheng, H., Fleitmann, D., Edwards, R. L., Wang, X., Cruz, F. W., Auler, A. S., Mangini, A., Wang, Y., Kong, X., Burns, S. J., and Matter, A.: Timing and structure of the 8.2 kyr B.P. event inferred from δ^{18}O records of stalagmites from China, Oman, and Brazil, Geology, 37, 1007–1010, https://doi.org/10.1130/G30126A.1, 2009.

Cheng, H., Sinha, A., Wang, X., Cruz, F. W., and Edwards, R. L.: The Global Paleomonsoon as seen through speleothem records from Asia and the Americas, Clim. Dynam., 39, 1045–1062, https://doi.org/10.1007/s00382-012-1363-7, 2012.

Clemens, S., Prell, W., Murray, D., Shimmield, G., and Weedon, G.: Forcing mechanisms of the Indian Ocean monsoon, Nature, 353, 720–725, 1991.

Clemens, S. C. and Prell, W. L.: A 350,000 year summer-monsoon multi-proxy stack from the Owen Ridge, Northern Arabian Sea, Mar. Geol., 201, 35–51, https://doi.org/10.1016/S0025-3227(03)00207-X, 2003.

Clift, P. D. and Plumb, R. A.: The Asian monsoon: causes, history and effects, Cambridge University Press, 270 pp., ISBN 978-0-521-84799-5, 2008.

Dahl, K. A. and Oppo, D. W.: Sea surface temperature pattern reconstructions in the Arabian Sea, Paleoceanography, 21, PA1014, https://doi.org/10.1029/2005PA001162, 2006.

Dallmeyer, A., Claussen, M., Wang, Y., and Herzschuh, U.: Spatial variability of Holocene changes in the annual precipitation pattern: A model-data synthesis for the Asian monsoon region, Clim. Dynam., 40, 2919–2936, https://doi.org/10.1007/s00382-012-1550-6, 2013.

Dallmeyer, A., Claussen, M., Lorenz, S. J., and Shanahan, T.: The end of the African humid period as seen by a transient comprehensive Earth system model simulation of the last 8000 years, Clim. Past, 16, 117–140, https://doi.org/10.5194/cp-16-117-2020, 2020.

Dansgaard, W., Johnsen, S. J., Clausen, H. B., Dahl-Jensen, D., Gundestrup, N. S., Hammer, C. U., Hvidberg, C. S., Steffensen, J. P., Sveinbjörnsdottir, A. E., and Jouzel, J.: Evidence for general instability of past climate from a 250-kyr ice-core record, Nature, 364, 218–220, https://doi.org/10.1038/364218a0, 1993.

De Boyer Montégut, C., Vialard, J., Shenoi, S. S. C., Shankar, D., Durand, F., Ethé, C., and Madec, G.: Simulated seasonal and interannual variability of the mixed layer heat budget in the northern Indian Ocean, J. Climate, 3249–3268, https://doi.org/10.1175/JCLI4148.1, 2007.

de Marez, C., L'Hégaret, P., Morvan, M., and Carton, X.: On the 3D structure of eddies in the Arabian Sea, Deep-Sea Res. Pt. I, 150, 103057, https://doi.org/10.1016/j.dsr.2019.06.003, 2019.

Demenocal, P., Ortiz, J., Guilderson, T., Adkins, J., Sarnthein, M., Baker, L., and Yarusinsky, M.: Abrupt onset and termination of the African Humid Period: rapid climate responses to gradual insolation forcing, Quaternary Sci. Rev., 19, 347–361, 2000.

Deplazes, G., Lückge, A., Stuut, J. B. W., Pätzold, J., Kuhlmann, H., Husson, D., Fant, M., and Haug, G. H.: Weakening and strengthening of the Indian monsoon during Heinrich events and Dansgaard-Oeschger oscillations, Paleoceanography, 29, 99–114, https://doi.org/10.1002/2013PA002509, 2014.

Dixit, Y., Hodell, D. A., Sinha, R., and Petrie, C. A.: Abrupt weakening of the Indian summer monsoon at 8.2 kyr B.P., Earth Planet. Sc. Lett., 391, 16–23, https://doi.org/10.1016/j.epsl.2014.01.026, 2014.

Dong, C., Nencioli, F., Liu, Y., and McWilliams, J. C.: An automated approach to detect oceanic eddies from satellite remotely sensed sea surface temperature data, IEEE Geosci. Remote Sens. Lett., 8, 1055–1059, https://doi.org/10.1109/LGRS.2011.2155029, 2011.

Doose-Rolinski, H., Rogalla, U., Scheeder, G., Lückge, A., and von Rad, U.: High-resolution temperature and evaporation changes during the late Holocene in the Northeastern Arabian Sea, Paleoceanography, 16, 358–367, https://doi.org/10.1029/2000PA000511, 2001.

Duplessy, J. C.: Glacial to interglacial contrasts in the northern Indian Ocean, Nature, 295, 494–498, https://doi.org/10.1038/295494a0, 1982.

Dutt, S., Gupta, A. K., Clemens, S. C., Cheng, H., Singh, R. K., Kathayat, G., and Lawrence Edwards, R.: Abrupt changes in Indian summer monsoon strength during 33,800 to 5500 years B.P., Geophys. Res. Lett., 42, 5526–5532, https://doi.org/10.1002/2015GL064015, 2015.

Dykoski, C. A., Edwards, R. L., Cheng, H., Yuan, D., Cai, Y., Zhang, M., Lin, Y., Qing, J., An, Z., and Revenaugh, J.: A high-resolution, absolute-dated Holocene and deglacial Asian monsoon record from Dongge Cave, China, Earth Planet. Sc. Lett., 233, 71–86, https://doi.org/10.1016/j.epsl.2005.01.036, 2005.

Emery, W. J. and Meincke, J.: Global Water Masses: Summary and Review, Oceanol. Acta, 9, 383–391, 1986.

Fang, X.-M., Ono, Y., Fukusawa, H., Bao-Tian, P., Li, J.-J., Dong-Hong, G., Oi, K., Tsukamoto, S., Torii, M., and Mishima, T.: Asian summer monsoon instability during the past 60,000 years: magnetic susceptibility and pedogenic evidence from the western Chinese Loess Plateau, Earth Planet. Sc. Lett., 168, 219–232, 1999.

Findlater, B. J.: A major low-level air current near the Indian Ocean during the northern summer, Q. J. Roy. Meteorol. Soc., 95, 362–380, 1969.

Fischer, A. S., Weller, R. A., Rudnick, D. L., Eriksen, C. C., Lee, C. M., Brink, K. H., Fox, C. A., and Leben, R. R.: Mesoscale eddies, coastal upwelling, and the upper-ocean heat budget in the Arabian Sea, Deep-Sea Res. Pt. II, 49, 2231–2264, 2002.

Fleitmann, D., Burns, S. J., Mudelsee, M., Neff, U., Kramers, J., Mangini, A., and Matter, A.: Holocene Forcing of the Indian Monsoon Recorded in a Stalagmite from Southern Oman, Springer-Verlag, 1737–1739, https://doi.org/10.1126/science.1083130, 2003.

Fleitmann, D., Burns, S. J., Mangini, A., Mudelsee, M., Kramers, J., Villa, I., Neff, U., Al-Subbary, A. A., Buettner, A., Hippler, D., and Matter, A.: Holocene ITCZ and Indian monsoon dynamics recorded in stalagmites from Oman and Yemen (Socotra), Quaternary Sci. Rev., 26, 170–188, https://doi.org/10.1016/j.quascirev.2006.04.012, 2007.

Fleitmann, D., Cheng, H., Badertscher, S., Edwards, R. L., Mudelsee, M., Göktürk, O. M., Fankhauser, A., Pickering, R., Raible, C. C., Matter, A., Kramers, J., and Tüysüz, O.: Timing and climatic impact of Greenland interstadials recorded in stalagmites from northern Turkey, Geophys. Res. Lett., 36, L19707, https://doi.org/10.1029/2009GL040050, 2009.

Fuchs, M. and Buerkert, A.: A 20 ka sediment record from the Hajar Mountain range in N-Oman, and its implication for detecting arid-humid periods on the southeastern Arabian Peninsula, Earth Planet. Sc. Lett., 265, 546–558, https://doi.org/10.1016/j.epsl.2007.10.050, 2008.

Gadgil, S.: The Indian monsoon and its variability, Annu. Rev. Earth Planet. Sci., 31, 429–467, https://doi.org/10.1146/annurev.earth.31.100901.141251, 2003.

Ganopolski, A. and Rahmstorf, S.: Rapid changes of glacial climate simulated in a coupled climate model, Nature, 409, 153–158, 2001.

Gaye, B., Böll, A., Segschneider, J., Burdanowitz, N., Emeis, K.-C., Ramaswamy, V., Lahajnar, N., Lückge, A., and Rixen, T.: Glacial–interglacial changes and Holocene variations in Arabian Sea denitrification, Biogeosciences, 15, 507–527, https://doi.org/10.5194/bg-15-507-2018, 2018.

geoBoundaries: Shapefile data, https://www.geoboundaries.org/globalDownloads.html (last access: 9 February 2024), 2024.

Giesche, A., Staubwasser, M., Petrie, C. A., and Hodell, D. A.: Indian winter and summer monsoon strength over the 4.2 ka BP event in foraminifer isotope records from the Indus River delta in the Arabian Sea, Clim. Past, 15, 73–90, https://doi.org/10.5194/cp-15-73-2019, 2019.

Godad, S. P., Panmei, C., and Naidu, P. D.: Remote forcing of winter cooling in the Arabian Sea: Implications for the NE monsoon, Palaeogeogr. Palaeoclim. Palaeoecol., 586, 110755, https://doi.org/10.1016/j.palaeo.2021.110755, 2022.

Google Earth: Web map service (WMS) layer, https://mt1.google.com/vt/lyr=s&x=x&y=y&z=z (last access: 9 February 2024), 2024.

Gouhier, T. C., Grinsted, A., and Simko, V.: R package biwavelet: Conduct Univariate and Bivariate Wavelet Analyses, R package version 0.20.21, GitHub [code], https://github.com/tgouhier/biwavelet (last access: 8 August 2023), 2021.

Gupta, A. K., Prakasam, M., Dutt, S., Clift, P. D., and Yadav, R. R.: Evolution and development of the Indian monsoon, in: Springer Geology, Springer, 499–535, https://doi.org/10.1007/978-3-030-15989-4_14, 2020.

Heinrich, H.: Origin and consequences of cyclic ice rafting in the Northeast Atlantic Ocean during the past 130,000 years, Quatern. Res., 29, 142–152, https://doi.org/10.1016/0033-5894(88)90057-9, 1988.

Held, F., Cheng, H., Edwards, R. L., Tüysüz, O., Koç, K., and Fleitmann, D.: Dansgaard-Oeschger cycles of the penultimate and last glacial period recorded in stalagmites from Türkiye, Nat. Commun., 15, 1183, https://doi.org/10.1038/s41467-024-45507-5, 2024.

Hemming, S. R.: Heinrich events: Massive late Pleistocene detritus layers of the North Atlantic and their global climate imprint, Rev. Geophys., 42, RG1005, https://doi.org/10.1029/2003RG000128, 2004.

Herzschuh, U.: Palaeo-moisture evolution in monsoonal Central Asia during the last 50,000 years, Quaternary Sci. Rev., 25, 163–178, https://doi.org/10.1016/j.quascirev.2005.02.006, 2006.

Honjo, S., Dymond, J., Prell, W., and Ittekkot, V.: Monsoon-controlled export fluxes to the interior of the Arabian Sea, Deep[Sea Research Pt. II, 46, 1859–1902, 1999.

Huguet, C., Kim, J. H., Damsté, J. S. S., and Schouten, S.: Reconstruction of sea surface temperature variations in the Arabian Sea over the last 23 kyr using organic proxies (TEX_{86} and $U^{K'}_{37}$), Paleoceanography, 21, PA3003, https://doi.org/10.1029/2005PA001215, 2006.

Izumo, T., de Montegut, C. B., Luo, J. J., Behera, S. K., Masson, S., and Yamagata, T.: The role of the Western Arabian Sea upwelling in Indian monsoon rainfall variability, J. Climate, 21, 5603–5623, https://doi.org/10.1175/2008JCLI2158.1, 2008.

Jaglan, S., Gupta, A. K., Clemens, S. C., Dutt, S., Cheng, H., and Singh, R. K.: Abrupt Indian summer monsoon shifts aligned with Heinrich events and D–O cycles since MIS 3, Palaeogeogr. Palaeoclim. Palaeoecol., 583, 110658, https://doi.org/10.1016/j.palaeo.2021.110658, 2021.

Johnsen, S. J., Clausen, H. B., Dansgaard, W., Fuhrer, K., Gundestrup, N., Hammer, C. U., and Steffensen, J. P.: Irregular glacial interstadials recorded in a new Greenland ice core, Nature, 359, 311–313, 1992.

Kessarkar, P. M., Purnachadra Rao, V., Naqvi, S. W. A., and Karapurkar, S. G.: Variation in the Indian summer monsoon intensity during the Bølling-Ållerød and Holocene, Paleoceanography, 28, 413–425, https://doi.org/10.1002/palo.20040, 2013.

Krebs, U. and Timmermann, A.: Tropical air-sea interactions accelerate the recovery of the Atlantic Meridional Overturning Circulation after a major shutdown, J. Climate, 20, 4940–4956, https://doi.org/10.1175/JCLI4296.1, 2007.

Krishna Kumar, K., Rupa Kumar, K., Ashrit, R. G., Deshpande, N. R., and Hansen, J. W.: Climate impacts on Indian agriculture, Int. J. Climatol., 24, 1375–1393, https://doi.org/10.1002/joc.1081, 2004.

Kumar, S. P. and Prasad, T. G.: Winter cooling in the northern Arabian Sea, Science, 71, 834–841, 1996.

Kumar, S. P. and Prasad, T. G.: Formation and spreading of Arabian Sea high-salinity water mass, J. Geophys. Res.-Oceans, 104, 1455–1464, https://doi.org/10.1029/1998jc900022, 1999.

Lambeck, K.: Shoreline reconstructions for the Persian Gulf since the last glacial maximum, Earth Planet. Sc. Lett., 142, 43–57, 1996.

Lean, J.: Solar forcing of climate change in recent millennia, in: Climate Development and History of the North Atlantic Realm, edited by: Wefer, G., Berger, W., Behre, K.-E., and Jansen, E., Springer-Verlag, Berlin, 75–88, https://doi.org/10.1007/978-3-662-04965-5_6, 2002.

Leuschner, D. C. and Sirocko, F.: The low-latitude monsoon climate during Dansgaard-Oeschger cycles and Heinrich Events, Quaternary Sci. Rev., 19, 243–254, https://doi.org/10.1016/S0277-3791(99)00064-5, 2000.

Levitus, S. and Boyer, T.: World Ocean Atlas 1994, in: vol. 4. Temperature, NOAA Atlas NESDIS. US Department of Commerce, Washington, D.C., https://repository.library.noaa.gov/view/noaa/1381 (last access: 24 January 2024), 1994.

L'Hegaret, P., Carton, X., Louazel, S., and Boutin, G.: Mesoscale eddies and submesoscale structures of Persian Gulf Water off the Omani coast in spring 2011, Ocean Sci., 12, 687–701, https://doi.org/10.5194/os-12-687-2016, 2016.

Loutre, M. F., Berger, A., Bretagnon, P., and Blanc, P.-L.: Astronomical frequencies for climate research at the decadal to century time scale, Clim. Dynam., 7, 181–194, 1992.

Madhupratap, M., Prasanna Kumar, S., Bhattathiri, P. M. A., Dileep Kumar, M., Raghukumar, S., Nair, K. K. C., and Ramaiah, N.: Mechanism of the biological response to winter cooling in the northeastern Arabian Sea, Nature, 384, 549–552, 1996.

Mayewski, P. A., Meeker, L. D., Twickler, M. S., Whitlow, S., Yang, Q., Lyons, W. B., and Prentice, M.: Major features and forcing of high-latitude northern hemisphere atmospheric circulation using a 110,000-year-long glaciochemical series, J. Geophys. Res.-Oceans, 102, 26345–26366, https://doi.org/10.1029/96JC03365, 1997.

McManus, J. F., Francois, R., Gherardi, J.-M., Keigwin, L. D., and Brown-Leger, S.: Collapse and rapid resumption of Atlantic meridional circulation linked to deglacial climate changes, Nature, 428, 834–837, 2004.

Menzel, P., Gaye, B., Mishra, P. K., Anoop, A., Basavaiah, N., Marwan, N., Plessen, B., Prasad, S., Riedel, N., Stebich, M., and Wiesner, M. G.: Linking Holocene drying trends from Lonar Lake in monsoonal central India to North Atlantic cooling events, Palaeogeogr. Palaeoclim. Palaeoecol., 410, 164–178, https://doi.org/10.1016/j.palaeo.2014.05.044, 2014.

Naidu, P. D. and Malmgren, B. A.: A 2,200 years periodicity in the Asian Monsoon System, Geophys. Res. Lett., 22, 2361–2364, https://doi.org/10.1029/95GL02558, 1995.

Naidu, P. D. and Malmgren, B. A.: Seasonal sea surface temperature contrast between the Holocene and last glacial period in the western Arabian Sea (Ocean Drilling Project Site 723A): Modulated by monsoon upwelling, Paleoceanography, 20, 1–9, https://doi.org/10.1029/2004PA001078, 2005.

Naidu, P. D., Niitsuma, N., Thirumalai, K., and Naik, S. S.: Significant seasonal contrast in the Arabian Sea during deglaciation: Evidence from oxygen isotopic analyses of individual planktic foraminifera, Quatern. Int., 503, 163–169, https://doi.org/10.1016/j.quaint.2018.08.005, 2019.

Neff, U., Burns, S. J., Mangini, A., Mudelsee, M., Fleitmann, D., and Matter, A.: Strong coherence between solar variability and the monsoon in Oman between 9 and 6 kyr ago, Nature, 411, 290–293, 2001.

Overpeck, J., Anderson, D., Trumbore, S., and Prell, W.: The southwest Indian Monsoon over the last 18 000 years, Clim. Dynam., 12, 213–225, 1996.

Pathak, V. K., Kharwar, A., and Rai, A. K.: Benthic foraminiferal response to changes in the northwestern Arabian Sea oxygen minimum zone (OMZ) during past ∼ 145 kyr, J. Earth Syst. Sci., 130, 163, https://doi.org/10.1007/s12040-021-01659-2, 2021.

Pedro, J. B., Andersson, C., Vettoretti, G., Voelker, A. H. L., Waelbroeck, C., Dokken, T. M., Jensen, M. F., Rasmussen, S. O., Sessford, E. G., Jochum, M., and Nisancioglu, K. H.: Dansgaard-Oeschger and Heinrich event temperature anomalies in the North Atlantic set by sea ice, frontal position and thermocline structure, Quaternary Sci. Rev., 289, 107599, https://doi.org/10.1016/j.quascirev.2022.107599, 2022.

Piontkovski, S. A., Hamza, W. M., Al-Abri, N. M., Al-Busaidi, S. S. Z., and Al-Hashmi, K. A.: A comparison of seasonal variability of Arabian Gulf and the Sea of Oman pelagic ecosystems, Aquat. Ecosyst. Health Manage., 22, 108–130, https://doi.org/10.1080/14634988.2019.1621133, 2019.

Pous, S. P., Carton, X., and Lazure, P.: Hydrology and circulation in the Strait of Hormuz and the Gulf of Oman – Results from the GOGP99 Experiment: 2. Gulf of Oman, J. Geophys. Res., 109, 57–78, https://doi.org/10.1029/2003jc002146, 2004.

Prahl, F. G., Muehlhausen, L. A., and Zahnle, D. L.: Further evaluation of long-chain alkenones as indicators of paleoceanographic conditions, Geochim. Cosmochim. Ac., 52, 2303–2310, https://doi.org/10.1016/0016-7037(88)90132-9, 1988.

Prasad, T. G. and Ikeda, M.: The Wintertime Water Mass Formation in the Northern Arabian Sea: A Model Study, J. Phys. Oceanogr., 32, 1028–1040, 2002.

Prasad, T. G., Ikeda, M., and Kumar, S. P.: Seasonal spreading of the Persian Gulf Water mass in the Arabian Sea, J. Geophys. Res.-Oceans, 106, 17059–17071, https://doi.org/10.1029/2000jc000480, 2001.

Prell, W. L. and Kutzbach, J. E.: Sensitivity of the Indian monsoon to forcing parameters and implications for its evolution, Nature, 360, 647–652, 1992.

Prell, W. L. and van Campo, E.: Coherent response of Arabian Sea upwelling and pollen transport to late Quaternary monsoonal winds, Nature, 323, 526–528, https://doi.org/10.1038/323526a0, 1986.

Premchand, K., Sastry, J. S., and Murty, C. S.: Water mass structure in the western Indian Ocean, II: The spreading and transportation of Persian Gulf water, Mausam, 37, 179–186, 1986.

Rasmussen, S. O., Bigler, M., Blockley, S. P., Blunier, T., Buchardt, S. L., Clausen, H. B., Cvijanovic, I., Dahl-Jensen, D., Johnsen, S. J., Fischer, H., Gkinis, V., Guillevic, M., Hoek, W. Z., Lowe, J. J., Pedro, J. B., Popp, T., Seierstad, I. K., Steffensen, J. P., Svensson, A. M., Vallelonga, P., Vinther, B. M., Walker, M. J. C., Wheatley, J. J., and Winstrup, M.: A stratigraphic framework for abrupt climatic changes during the Last Glacial period based on three synchronized Greenland ice-core records: Refining and extending the INTIMATE event stratigraphy, Quaternary Sci. Rev., 106, 14–28, https://doi.org/10.1016/j.quascirev.2014.09.007, 2014.

R Core Team: R: A Language and Environment for Statistical Computing, https://www.r-project.org/ (last access: 16 May 2023), 2023.

Reichart, G. J., Lourens, L. J., and Zachariasse, W. J.: Temporal variability in the northern Arabian Sea oxygen minimum zone (OMZ) during the last 225,000 years, Paleoceanography, 13, 607–621, https://doi.org/10.1029/98PA02203, 1998.

Reimer, P. J. and Reimer, R. W.: A Marine Reservoir Correction Database and On-Line Interface, Radiocarbon, 43, 461–463, https://doi.org/10.1017/S0033822200038339, 2001.

Resplandy, L., Lévy, M., Bopp, L., Echevin, V., Pous, S., Sarma, V. V. S. S., and Kumar, D.: Controlling factors of the oxygen balance in the Arabian Sea's OMZ, Biogeosciences, 9, 5095–5109, https://doi.org/10.5194/bg-9-5095-2012, 2012.

Rixen, T., Ittekkot, V., Haake-Gaye, B., and Schak, P.: The infuence of the SW monsoon on the deep-sea organic carbon cycle in the Holocene, Deep-Sea Res. Pt. II, 47, 2629–2651, 2000.

Rochford, D. J.: Salinity maxima in the upper 1000 metres of the north Indian Ocean, Mar. Freshwater Res., 15, 1–24, 1964.

Rostek, F., Bard, E., Beaufort, L., Sonzogni, C., and Ganssen, G.: Sea surface temperature and productivity records for the past 240 kyr in the Arabian Sea, Deep-Sea Res. Pt. II, 44, 1461–1480, https://doi.org/10.1016/S0967-0645(97)00008-8, 1997.

Saher, M. H., Jung, S. J. A., Elderfield, H., Greaves, M. J., and Kroon, D.: Sea surface temperatures of the western Arabian Sea during the last deglaciation, Paleoceanography, 22, PA2208, https://doi.org/10.1029/2006PA001292, 2007.

Schneider, T., Bischoff, T., and Haug, G. H.: Migrations and dynamics of the intertropical convergence zone, Nature, 513, 45–53, https://doi.org/10.1038/nature13636, 2014.

Schott, F. A., Dengler, M., and Schoenefeldt, R.: The shallow overturning circulation of the Indian Ocean, Prog. Oceanogr., 53, 57–103, 2002.

Schulte, S. and Müller, P. J.: Variations of sea surface temperature and primary productivity during Heinrich and Dansgaard-Oeschger events in the Northeastern Arabian Sea, Geo-Mar. Lett., 21, 168–175, https://doi.org/10.1007/s003670100080, 2001.

Schulte, S., Rostek, F., Bard, E., Rullkötter, J., and Marchal, O.: Variations of oxygen-minimum and primary productivity recorded in sediments of the Arabian Sea, Earth Planet. Sc. Lett., 173, 205–221, 1999.

Schulz, H., van Rad, U., and Erlenkeuser, H.: Correlation between Arabian Sea and Greenland climate oscillations of the past 110,000 years, Nature, 292, 54–57, 1998.

Schulz, M. and Mudelsee, M.: REDFIT: estimating red-noise spectra directly from unevenly spaced paleoclimatic time series, Comput. Geosci., 28, 421–426, 2002.

Sheng Hu, F., Kaufman, D., Yoneji, S., Nelson, D., Shemesh, A., Huang, Y., Tian, J., Bond, G., Clegg, B., and Brown, T.: Cyclic Variation and Solar Forcing of Holocene Climate in the Alaskan Subarctic, Science, 301, 1890–1893, 2003.

Shetye, S. R., Gouveia, A. D., and Shenoi, S. S. C.: Circulation and water masses of the Arabian Sea, Proc. Indian Acad. Sci. (Earth Planet. Sci.), 103, 107–123, 1994.

Sirocko, F. and Lange, H.: Clay-mineral accumulation rates in the Arabian Sea during the late Quaternary, Mar. Geol., 97, 105–119, 1991.

Sirocko, F. and Sarnthein, M.: Wind-Borne Deposits in the Northwestern Indian Ocean: Record of Holocene Sediments Versus Modern Satellite Data, in: Paleoclimatology and Paleometeorology: Modern and Past Patterns of Global Atmospheric Transport, Springer, Dordrecht, 401–433, https://doi.org/10.1007/978-94-009-0995-3_17, 1989.

Sirocko, F., Sarnthein, M., Lange, H., and Erlenkeuser, H.: Atmospheric summer circulation and coastal upwelling in the Arabian Sea during the Holocene and the last glaciation, Quatern. Res., 36, 72–93, 1991.

Sirocko, F., Garbe-Schönberg, D., Mclntyre, A., and Molfino, B.: Teleconnections Between the Subtropical Monsoons and High-Latitude Climates During the Last Deglaciation, Science, 272, 526–529, 1996.

Sirocko, F., Garbe-Schonberg, D., and Devey, C.: Processes controlling trace element geochemistry of Arabian Sea sediments during the last 25,000 years, Global Planet. Change, 26, 217–303, 2000.

Sonzogni, C., Bard, E., Rostek, F., Lafont, R., Rosell-Melets, A., and Eglinton, G.: Core-top calibration of the alkenone index vs sea surface temperature in the Indian Ocean, Deep-Sea Res. Pt. II, 44, 1445–1460, 1997.

Southon, J.: Evidence for persistent 7000- and 3500-year geomagnetic oscillations, Geophys. Res. Lett., 29, 61, https://doi.org/10.1029/2002GL014734, 2002.

Southon, J., Kashgarian, M., Fontugne, M., Metivier, B., and Yim, W.-S.: Marine Reservoir Corrections for the Indian Ocean and Southeast Asia, Radiocarbon, 44, 167–180, https://doi.org/10.1017/S0033822200064778, 2002.

Struiver, M. and Brazinuas, T. F.: Sun, ocean, climate and atmospheric $^{14}CO_2$: an evaluation of causal and spectral relationships, Holocene, 3, 289–305, 1993.

Svensson, A., Andersen, K. K., Bigler, M., Clausen, H. B., Dahl-Jensen, D., Davies, S. M., Johnsen, S. J., Muscheler, R., Parrenin, F., Rasmussen, S. O., Röthlisberger, R., Seierstad, I., Steffensen, J. P., and Vinther, B. M.: A 60 000 year Greenland stratigraphic ice core chronology, Clim. Past, 4, 47–57, https://doi.org/10.5194/cp-4-47-2008, 2008.

Thamban, M., Kawahata, H., and Purnachandra Rao, V.: Indian Summer Monsoon Variability during the Holocene as Recorded in Sediments of the Arabian Sea: Timing and Implications, J. Oceanogr., 63, 1009–1020, 2007.

Tierney, J. E. and deMenocal, P. B.: Abrupt Shifts in Horn of Africa Hydroclimate Since the Last Glacial Maximum, Science, 342, 843–846, https://doi.org/10.1126/science.1244809, 2013.

Tierney, J. E., Pausata, F. S. R., and Demenocal, P.: Deglacial Indian monsoon failure and North Atlantic stadials linked by Indian Ocean surface cooling, Nat. Geosci., 9, 46–50, https://doi.org/10.1038/ngeo2603, 2016.

Tierney, J. E., Pausata, F. S. R., and Demenocal, P. B.: Rainfall regimes of the Green Sahara, Sci. Adv., 3, e1601503, https://doi.org/10.1126/sciadv.1601503, 2017.

Torrence, C. and Compo, G. P.: A Practical Guide to Wavelet Analysis, B. Am. Meteorol. Soc., 79, 61–78, 1998.

Trenberth, K. E., Dai, A., Rasmussen, R. M., and Parsons, D. B.: The changing character of precipitation, B. Am. Meteorol. Soc., 84, 1205–1218, https://doi.org/10.1175/BAMS-84-9-1205, 2003.

Trott, C. B., Subrahmanyam, B., Chaigneau, A., and Roman-Stork, H. L.: Eddy-Induced Temperature and Salinity Variability in the Arabian Sea, Geophys. Res. Lett., 46, 2734–2742, https://doi.org/10.1029/2018GL081605, 2019.

Vic, C., Roullet, G., Capet, X., Carton, X., Molemaker, M. J., and Gula, J.: Eddy-topography interactions and the fate of the Persian Gulf Outflow, J. Geophys. Res.-Oceans, 120, 6700–6717, https://doi.org/10.1002/2015JC011033, 2015.

Wang, Y., Cheng, H., Edwards, R. L., An, Z. S., Wu, J. Y., Shen, C. C., and Dorale, J. A.: A High-Resolution Absolute-Dated Late Pleistocene Monsoon Record from Hulu Cave, China, Science, 294, 2345–2348, https://doi.org/10.1126/science.1064618, 2001.

Watanabe, T. K., Watanabe, T., Yamazaki, A., Pfeiffer, M., Garbe-Schönberg, D., and Claereboudt, M. R.: Past summer upwelling events in the Gulf of Oman derived from a coral geochemical record, Sci. Rep., 7, 4568, https://doi.org/10.1038/s41598-017-04865-5, 2017.

Webster, P. J.: Dynamics of the tropical atmosphere and oceans, John Wiley & Sons, Ltd., https://doi.org/10.1002/9781118648469, 2020.

Webster, P. J., Magaña, V. O., Palmer, T. N., Shukla, J., Tomas, R. A., Yanai, M., and Yasunari, T.: Monsoons: processes, predictability, and the prospects for prediction, J. Geophys. Res.-Oceans, 103, 14451–14510, https://doi.org/10.1029/97jc02719, 1998.

Wyrtki, K.: Physical Oceanography of the Indian Ocean, in: The Biology of the Indian Ocean, Springer, Berlin, Heidelberg, 18–36, https://doi.org/10.1007/978-3-642-65468-8_3, 1973.

Yao, F. and Johns, W. E.: A HYCOM modeling study of the Persian Gulf: 1. Model configurations and surface circulation, J. Geophys. Res.-Oceans, 115, C11017, https://doi.org/10.1029/2009JC005781, 2010.

You, Y.: Intermediate water circulation and ventilation of the Indian Ocean derived from water-mass contributions, J. Mar. Res., 56, 1029–1067, https://doi.org/10.1357/002224098765173455, 1998.

Yue, X., Liao, H., Wang, H. J., Li, S. L., and Tang, J. P.: Role of sea surface temperature responses in simulation of the climatic effect of mineral dust aerosol, Atmos. Chem. Phys., 11, 6049–6062, https://doi.org/10.5194/acp-11-6049-2011, 2011.

Zhang, R. and Delworth, T. L.: Simulated Tropical Response to a Substantial Weakening of the Atlantic Thermohaline Circulation, J. Climate, 18, 1853–1860, 2005.

Zhou, W., Head, M. J., Lu, X., An, Z., Jull, A. J. T., and Donahue, D.: Teleconnection of climatic events between East Asia and polar, high latitude areas during the last deglaciation, Palaeogeogr. Palaeoclim. Palaeoecol., 152, 163–172, 1999.